Structure of p-shell nuclei using three-nucleon interactions evolved with the similarity renormalization group

E. D. Jurgenson, P. Maris, R. J. Furnstahl, P. Navrátil, W. E. Ormand, and J. P. Vary

Structure of p-shell nuclei using three-nucleon interactions evolved with the similarity renormalization group

E.D. Jurgenson,[1, *] P. Maris,[2, †] R.J. Furnstahl,[3, ‡] P. Navrátil,[4, §] W.E. Ormand,[1, ¶] and J.P. Vary[2, **]

[1]*Lawrence Livermore National Laboratory, P.O. Box 808, L-414, Livermore, CA 94551, USA*
[2]*Department of Physics and Astronomy, Iowa State University, Ames, IA 50011, USA*
[3]*Department of Physics, The Ohio State University, Columbus, OH 43210, USA*
[4]*TRIUMF, 4004 Westbrook Mall, Vancouver, BC, V6T 2A3, Canada*
(Dated: April 7, 2013)

The Similarity Renormalization Group (SRG) is used to soften interactions for *ab initio* nuclear structure calculations by decoupling low- and high-energy Hamiltonian matrix elements. The substantial contribution of both initial and SRG-induced three-nucleon forces requires their consistent evolution in a three-particle basis space before applying them to larger nuclei. While in principle the evolved Hamiltonians are unitarily equivalent, in practice the need for basis truncation introduces deviations, which must be monitored. Here we present benchmark no-core full configuration calculations with SRG-evolved interactions in p-shell nuclei over a wide range of softening. These calculations are used to assess convergence properties, extrapolation techniques, and the dependence of energies, including four-body contributions, on the SRG resolution scale.

I. INTRODUCTION

Configuration interaction methods have been used in recent years to make increasingly accurate large scale *ab initio* calculations of nuclear structure and reactions (e.g., see Refs. [1–6]) Improved algorithms and better use of increasing computational resources are critical for these successes. However, the reach of these methods may also be extended by applying renormalization group (RG) transformations to the input Hamiltonian. Renormalization techniques soften the free-space interactions by reducing the coupling between high and low momenta, leading to improved convergence with the size of the basis for a fixed number of interacting nucleons. The Similarity Renormalization Group (SRG) [7, 8] is an attractive approach for this purpose due to its relatively simple implementation, general flexibility, and the feasibility of consistently evolving many-body operators [9, 10].

Previous studies of the SRG in nuclear physics established its usefulness for few-body systems by demonstrating improved convergence with two-nucleon (NN) interactions alone [11–13]. In Ref. [14], a detailed study of SRG convergence with NN forces in the p-shell was made. The present work extends this study to include initial and induced three-nucleon (NNN) forces. We build upon the technology to evolve NNN forces introduced in Ref. [15], which was applied in Ref. [16] to ^{4}He and ^{6}Li to explore the effects of full two-plus-three-body evolved interactions in light nuclei. Roth et al. have subsequently used the Importance Truncated No-Core Shell Model (IT-NCSM) with the SRG [17] to significantly push the limits in A and model space size [18, 19]. We focus here on a wider set of p-shell nuclei and on wider ranges of softening that, with our extrapolation methods, yield nearly converged results without implementing importance truncation.

The SRG flow equations generate a continuous series of Hamiltonians that is analogous to the running of the strong coupling constant in quantum chromodynamics, having both scale (or resolution) and scheme dependence [10]. The scheme dependence arises from the choice of initial nuclear Hamiltonian and the choice of the operator generating the flow (see below). While the SRG offers a useful framework for future comparisons of such choices for both NN and NNN interactions and exploring the flow to universal forms [9, 20], in this work, we restrict our attention to just one choice. In particular, we use the chiral effective field theory (EFT) potential at N^{3}LO with 500 MeV cutoff from Ref. [21] together with an NNN potential at N^{2}LO [22] in the local form of Ref. [23]. This is also the Hamiltonian used in Refs. [15, 16, 18, 24].

The scale dependence arising from the RG flow is manifested as a decreasing decoupling scale that marks the energy difference for which matrix elements between off-diagonal energy states become highly suppressed. Formally, all of the evolved Hamiltonians have equivalent physics content to that of the initial Hamiltonian, so it would seem to be advantageous to evolve to very low scales to optimize the convergence of many-body calculations. But in practice, the initial and running Hamiltonians are expanded in a finite basis (harmonic oscillators here) and many-body forces are truncated at some level. Therefore, it is necessary to monitor and characterize the evolution of many-body forces and the residual running of calculated observables, which can vary with the size of the nuclear system. In this paper, we present bench-

* jurgenson2@llnl.gov
† pmaris@iastate.edu
‡ furnstahl.1@osu.edu
§ navratil@triumf.ca
¶ ormand1@llnl.gov
** jvary@iastate.edu

mark calculations using SRG-evolved interactions in p-shell nuclei. We use them to explore the characteristics and practical limits of SRG evolution for these systems by assessing convergence properties, extrapolation techniques, and the stability of predicted observables.

In Section II, we briefly review the formalism used in this study and summarize some observations from previous work. A more complete discussion is provided in [16]. The convergence properties of the evolved NN and NNN potentials in various nuclei are explored in Section III and in Section IV we examine the evolution with λ and the patterns of induced many-body forces. Section V summarizes our conclusions and provides an outlook for future calculations.

II. BACKGROUND

A. SRG evolution

The SRG for low-energy nuclear physics generates a continuous series of Hamiltonians H_λ from an initial free-space Hamiltonian $H_{\lambda=\infty}$ by unitary transformations,

$$H_\lambda = U_\lambda H_{\lambda=\infty} U_\lambda^\dagger , \qquad (1)$$

which is carried out by solving a set of flow equations,

$$\frac{dH_\lambda}{d\lambda} = -\frac{4}{\lambda^5}[[G, H_\lambda], H_\lambda] . \qquad (2)$$

With an appropriate choice of the hermitian operator G, the Hamiltonian is evolved to band-diagonal form with respect to energy [8, 25]. In most nuclear applications to date, the relative kinetic energy $T_{\rm rel}$ has been used because of the favorable convergence properties of the evolved Hamiltonians and for its convenience in constructing basis expansions [9, 10]. We use it here exclusively but note that other choices may be advantageous in reducing the growth of many-body forces. This is being investigated separately [26, 27]. The flow parameter λ keeps track of the sequence of Hamiltonians (s or α, with $s = \alpha = 1/\lambda^4$, are also used elsewhere [11, 12, 18]). For $G = T_{\rm rel}$, λ has dimensions of momentum and runs from ∞ toward zero with increasing softening.

Evolution is performed in the Jacobi-coordinate harmonic oscillator (HO) basis used for the No-Core Shell Model (NCSM) [2, 6]. This is a translationally invariant, anti-symmetric basis for each A-body sector, in which a complete set of states in the model space is defined by the maximum excitation of $N_{\max}\hbar\Omega$ above the minimum energy configuration, where Ω is the harmonic oscillator parameter. This basis is variational in $N_{\max}$; that is, the energy converges asymptotically from above as more basis states are included. The SRG preserves this variational characteristic through smooth unitary evolution, in contrast to Okubo-Lee-Suzuki based renormalizations [2, 6], which are unitary transformations specific to the model space.

TABLE I. Definitions and values of basis-size truncations used on the initial Hamiltonian and on the model space for the CI calculations. The value of $N_{\rm A3max}$ is uniformly reduced for three-body partial-wave JπT channels with higher J to a minimum of 20.

$N_{\rm A2max}$	Maximum sum of two-body oscillator quanta for initial two-body matrix element evolution	300
$N_{\rm A3max}$	Maximum sum of three-body oscillator quanta for initial three-body matrix element evolution	40
$N_{\max}$	Maximum sum of A-body oscillator quanta above the minimum for the A-body system	2–8

We start by evolving H_λ using Eq. (2) in the $A = 2$ subsystem, completely fixing the evolved two-body matrix elements. Next, by evolving H_λ in the $A = 3$ subsystem we determine the combined two-plus-three-body matrix elements. We isolate the three-body matrix elements by subtracting the evolved two-body elements within the $A = 3$ basis [28]. Having obtained the separate NN and NNN matrix elements we can apply them as inputs to any *ab initio* nuclear structure problem. We are also free to include an initial three-nucleon force in the starting Hamiltonian without changing the procedure.

While any initial interaction can be used as input to the SRG evolution, here we use the chiral EFT NN potential from the 500 MeV N³LO interaction of Ref. [21] exclusively. As an initial NNN potential, we use the chiral N²LO potential [22] in the local form of Ref. [23]. The low-energy constants $c_D = -0.2$ and $c_E = -0.205$ are the result of a fit to the average of triton and ³He binding energies and to triton beta decay as described in Ref. [29].

Hamiltonians obtained via free-space SRG evolution are independent of the basis choice if the basis is sufficiently complete. That is, a Hamiltonian evolved to a given λ reproduces the results of a Hamiltonian evolved to the same λ in a different basis. But in practice there are truncations, both in A-body forces and in basis size, that are relevant to controlling the quality and consistency of SRG-evolved interactions.

In the present work, induced four-body (and higher) forces are not included, so calculations for $A \geq 4$ will be only approximately unitary. The many-body interaction matrix elements induced by the evolution appear in a decreasing hierarchy in few-body nuclei [15, 16]. One of our goals is to determine if that hierarchy is maintained for p-shell nuclei or if the induced many-body contributions become unnaturally large for certain systems and/or values of λ.

Because of computational constraints, we are forced to apply separate truncations to the $A = 2$ and $A = 3$ sectors of the initial Hamiltonian, which we denote $N_{\rm A2max}$ and $N_{\rm A3max}$, respectively (see Table I). These cutoffs in the basis size must be large enough to fully accommodate

the ultraviolet (UV) contributions (or high-momentum components) from the initial NN plus NNN Hamiltonian. The ultraviolet cutoff in an oscillator basis scales like $\sqrt{N\hbar\Omega}$, where N represents the maximum number of single-particle oscillator quanta in the basis, so there will be an $\hbar\Omega$ below which the initial and, therefore, evolved Hamiltonian projections onto the oscillator basis are incomplete. When we use such an $\hbar\Omega$ that is too low, we are effectively working with a different Hamiltonian. As a consequence, the calculations of observables in the many-body basis with the too-low $\hbar\Omega$ will not converge (or extrapolate) to the same results found at larger $\hbar\Omega$. This is not a problem for the NN interaction, for which N_{A2max} is sufficiently large for the chiral EFT Hamiltonian for all $\hbar\Omega$ considered, but becomes a factor for the NNN force, as illustrated below.

Hamiltonians are derived and evolved in the Jacobi basis for $A = 2$ and 3 and then translated to a Slater determinant basis for full configuration interaction (CI) calculations of larger systems. The particular CI procedure used here, including the extrapolation to infinite basis size and associated uncertainty estimates, is referred to as no-core full configuration or NCFC [1]. Other CI calculations in the literature using SRG-evolved interactions and extrapolation are called NCSM (e.g., Refs. [15, 16]). While the original NCSM featured a finite matrix truncation and an effective Hamiltonian renormalized to that finite space [6], these SRG-based NCSM and NCFC procedures are equivalent except for variations in the extrapolation and uncertainty quantification procedures.

In these CI calculations, the size of the largest feasible model space is highly constrained by the total number of two- and three-body matrix elements in the full space. Fortunately, the MFDn code [30–32] that carries out the Lanczos matrix diagonalization algorithm is highly optimized for parallel computing. The calculations were performed on the Intel Xeon cluster Sierra at LLNL, using up to about 15 TB of memory across 7,200 cores on the Cray XE6 Hopper at NERSC, using up to about 100 TB of memory across 76,320 cores; and on the Cray XK6 Jaguar at ORNL, using over 500 TB of memory across 261,120 cores. MFDn has been demonstrated to scale well on these platforms for these types of runs [33].

B. Guide to the calculations

To set the stage for our examination of p-shell nuclei, we show in Fig. 1 the ground-state energy of ^{4}He as a function of λ [15, 16]. Here, and throughout the paper, we will compare three types of calculations, which are summarized in Table II. The NN-only calculations include two-body matrix elements that are phase-shift equivalent to the initial NN interaction. When this part of the Hamiltonian is used alone to study $A > 2$ systems, the results are not unitarily equivalent at different λ because the SRG has reorganized the degrees of freedom to reduce coupling of high- and low-energies.

TABLE II. Guide to the calculations.

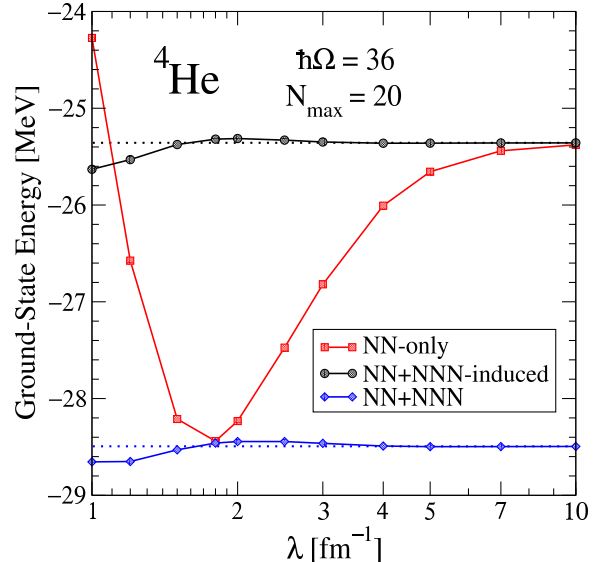| NN-only	No initial NNN interaction and do not keep NNN-induced interaction.
NN + NNN-induced	No initial NNN interaction but keep the SRG-induced NNN interaction arising from the NN interaction alone.
NN + NNN	Include an initial NNN interaction *and* keep the SRG-induced NNN interaction arising from the combination of NN and NNN interactions.

FIG. 1. (color online) Ground-state energy of ^{4}He as a function of λ for the three calculations in Table II. The results at all λ are converged at the 2 keV level or better. The dotted line is the unevolved result.

Formally, in the process of maintaining unitary equivalence in all sectors the SRG induces new contributions to many-body matrix elements, but in the NN-only result these induced interactions are omitted. We get a characteristic pattern (see the NN-only results in Fig. 1) where the converged result varies with evolution, starting at some (underbound) level for the initial Hamiltonian, then falling and rising again with subsequent evolution (decreasing λ).

In the NN+NNN-induced calculations, the Hamiltonian includes the evolved NN matrix elements as well as all three-body matrix elements induced by the SRG starting from only an NN interaction (i.e., no initial NNN). In an $A = 3$ system this will be unitarily equivalent to the initial NN-only Hamiltonian, so the energy spectrum will be the same, up to numerical truncation errors (e.g., because of an insufficient N_{A3max}). Finally, the NN+NNN calculations include an initial three-body interaction as well as the induced three-body matrix elements that now arise from the combined evolution of the NN+NNN in-

teractions. For $A = 3$, it should be unitarily equivalent to the initial NN+NNN Hamiltonian. For $A \geq 4$, there will be induced four-body (and higher-body) interactions that are not included in any of the present calculations. Their omission causes differences in the predicted energy spectra as a function of λ.

The computed ground-state energies for ^{4}He in Fig. 1 are well converged at all λ, so the interpretation is clear. For the NN-only calculations, deviations from unitary equivalence are evident just below $\lambda = 10\,\mathrm{fm}^{-1}$, where binding is increasing by a maximum of about three MeV (10% of the total binding energy), peaking just below $\lambda = 2\,\mathrm{fm}^{-1}$ and then decreasing rapidly and overshooting the original ground-state energy by $\lambda = 1\,\mathrm{fm}^{-1}$. A similar pattern for NN-only was shown in Ref. [14] for several p-shell nuclei.

The NN+NNN-induced calculation shows a dramatic reduction in the variation of the energy for $\lambda > 1.5\,\mathrm{fm}^{-1}$, with only a small decrease in the binding energy peaking near $\lambda = 2\,\mathrm{fm}^{-1}$. The deviations near $\lambda = 1\,\mathrm{fm}^{-1}$, which imply net induced four-body interaction contributions, are only about $300\,\mathrm{keV}$, or still an order of magnitude reduced from the largest NN-only variations. The same pattern for the (implied) induced four-body interaction is seen when an initial NNN interaction is included, with just a slight change in the pattern at $\lambda = 1\,\mathrm{fm}^{-1}$. When we compare to the larger nuclei in the present work, we will not be able to examine the full range of λ used in Fig. 1 because convergence is only sufficient for reliable extrapolation with small errors for λ up to about $2\,\mathrm{fm}^{-1}$.

C. Extrapolation methods

For well-evolved Hamiltonians in lighter nuclei (e.g., ^{3}H or ^{4}He at $\lambda \leq 1.5\,\mathrm{fm}^{-1}$), our predictions for ground-state energies are well converged at computationally accessible values of $N_{\max}$. However, for larger nuclei and greater λ values we will need to extrapolate calculated energies to $N_{\max} = \infty$. To do so, we primarily use empirical extrapolation procedures based on those described in Refs. [1, 14, 16] but also compare to a new procedure from Ref. [34].

The empirical model used for ground-state energies is

$$E_{\alpha i} = E_\infty + A_\alpha\, e^{-b_\alpha N_{\alpha i}} \;, \tag{3}$$

where A_α and b_α are ($\hbar\Omega$ dependent) constants, $N_{\alpha i}$ are the $N_{\max}$ values, and α labels the $\hbar\Omega$ value. The goal is to determine the common parameter E_∞, which is the estimate for the ground-state energy extrapolated to $N_{\max} = \infty$. This can be cast as a one-dimensional constrained minimization problem with the function

$$g(E_\infty) = \sum_{\alpha, i} (\log(E_{\alpha i} - E_\infty) - a_\alpha - b_\alpha N_{\alpha i})^2 / \sigma_{\alpha i}^2 \;, \tag{4}$$

where the $\{a_\alpha\}$ and $\{b_\alpha\}$ are determined directly within the function g by invoking a constrained linear least-squares minimization routine. The constraint is the

bound $E_\infty \leqslant \min(\{E_{\alpha i}\})$, where $E_\infty < 0$ and "min" means "most negative". (One can also allow for weights depending on $N_{\max}$ and/or $\hbar\Omega$.)

In the present investigation, we have applied this extrapolation model for individual values of $\hbar\Omega$, determining error estimates as in "Extrapolation B" from Ref. [1], but also including several values of $\hbar\Omega$ in a constrained fit over a range where they are considered reliable. We emphasize that while this model has been generally successful when applied in NCFC calculations with SRG-evolved interactions, its validation is empirical rather than theoretical.

An alternative EFT-motivated approach to extrapolation is based on explicitly considering the ultraviolet (UV) and infrared (IR) cutoffs imposed by a truncated harmonic oscillator basis [34, 35]. This has led to a theoretically motivated IR correction formula and an empirical UV correction formula [34] in which the basic extrapolation variables are the effective hard-wall size L and the analogous cut-off in momentum, Λ_{UV}. In terms of the oscillator length $b \equiv \sqrt{\hbar/(m\Omega)}$, rough estimates of these variables are $\Lambda_{UV} \approx \sqrt{2(N + 3/2)}\hbar/b$ and $L \approx \sqrt{2(N + 3/2)}b$, where $N = N_{\max} + 1$ for p-shell nuclei [34, 35]. A formula combining both corrections (i.e., they are treated independently) takes the form [34]

$$E(\Lambda_{UV}, L) \approx E_\infty + B_0 e^{-2\Lambda_{UV}^2/B_1^2} + B_2 e^{-2k_\infty L} \;. \tag{5}$$

Note that this formula contains exponentials with arguments proportional to both N (from Λ_{UV}^2) and $\sqrt{N}$ (from L), in contrast to Eq. (3).

Following Ref. [34], we apply Eq. (5) with E_∞, B_0, B_1, B_2, and k_∞ treated as fit parameters that are determined from a simultaneous optimization to data at all $\hbar\Omega$, including the intermediate region where both IR and UV corrections are significant. It may be advantageous in general to isolate the IR or UV corrections by using only large $\hbar\Omega$ or small $\hbar\Omega$ results, respectively. However, most of the present calculations were made with $\hbar\Omega$ values close to the energy minimum, which means comparable UV and IR contributions [34]. (The exception is for very low λ, where UV convergence is reached for all $\hbar\Omega$ considered.) We also exploit a recent observation that the expressions for L and Λ_{UV} give more accurate energy corrections if we take $N \to N + 2$, which is particularly effective when $N_{\max}$ is small [36]. Thus we will use $N = (N_{\max}+1)+2 = N_{\max}+3$ for the calculations in Section III C. Equation (5) has been successfully applied to NN-only calculations from Ref. [14], but here we test it for the first time with three-body forces included.

III. CONVERGENCE

For fixed $N_{\max}$, both the UV and IR momentum cutoffs scale with $\sqrt{\hbar\Omega}$, which means that there is a trade-off: increasing $\hbar\Omega$ increases the ability to accommodate high-momentum components while decreasing the ability

to accomodate long-distance physics. The result is a familiar variational minimum with respect to $\hbar\Omega$. For NN-only calculations, it was observed in Ref. [14] that with decreasing SRG λ at fixed $N_{\max}$, the minimum systematically shifts to lower $\hbar\Omega$ and convergence becomes much more rapid. Here we examine if these observations are modified by the presence of a three-nucleon force (3NF) in NN+NNN-induced and NN+NNN calculations.

A. Size of three-body evolution basis

As noted earlier, the size $N_{A3\max}$ of the $A = 3$ basis we use to evolve the Hamiltonian before embedding in larger systems is limited by computational constraints. In Fig. 2, the impact on the calculated ground-state of the triton is shown for the unevolved interaction using different values of $N_{A3\max}$ with $\hbar\Omega$ ranging from 10 to 24 MeV. At each $\hbar\Omega$, the signal that $N_{A3\max}$ is sufficiently large is convergence of the ground-state energy, which is evident for $\hbar\Omega \geq 18$. In contrast, the systematic underbinding at lower $\hbar\Omega$ values with the $N_{A3\max}$ from Table I will be preserved when the Hamiltonian is evolved; in effect a different initial Hamiltonian will be used. The spread of points at fixed $\hbar\Omega$ and particularly the deviations at $N_{A3\max} = 40$ from the fully converged energy imply that low oscillator parameters (i.e., below $\hbar\Omega = 18$ MeV), will be unreliable for energy calculations in larger nuclei (because we cannot predict the degree of underbinding, as shown in Fig. 4 discussed below). In contrast, the size of the $A = 2$ basis used here is sufficient for convergence within 1 keV in the full range of $\hbar\Omega$ considered.
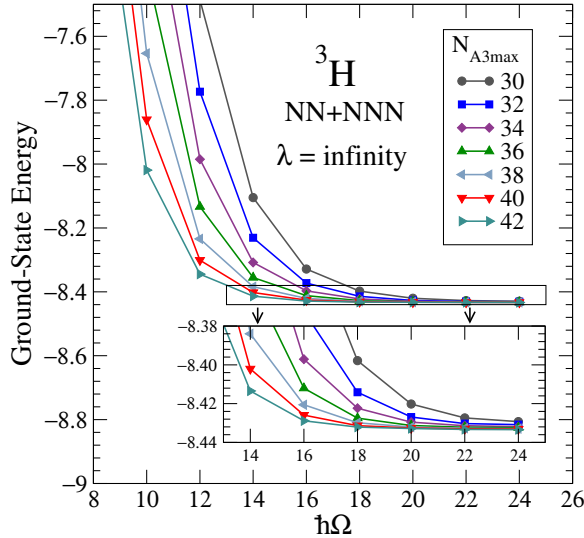

FIG. 2. (color online) Ground-state energy of the triton for the unevolved chiral EFT Hamiltonian in different three-body basis sizes ($N_{A3\max}$) with a large, fixed two-body basis ($N_{A2\max} = 300$).

The implications of a too-small $N_{A3\max}$ at smaller $\hbar\Omega$ for SRG evolution are illustrated in Fig. 3, which shows

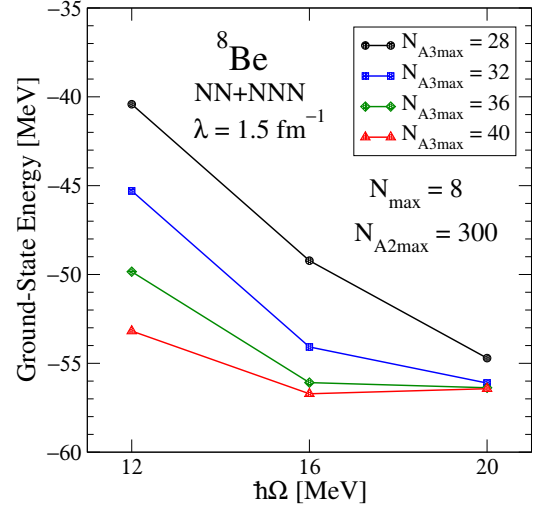FIG. 3. (color online) Ground-state energy of ^{8}Be for a fixed many-body basis size of $N_{\max} = 8$ for Hamiltonians evolved to $\lambda = 1.5\,\text{fm}^{-1}$ in different three-body basis sizes ($N_{A3\max}$) with a fixed, large two-body basis ($N_{A2\max} = 300$).
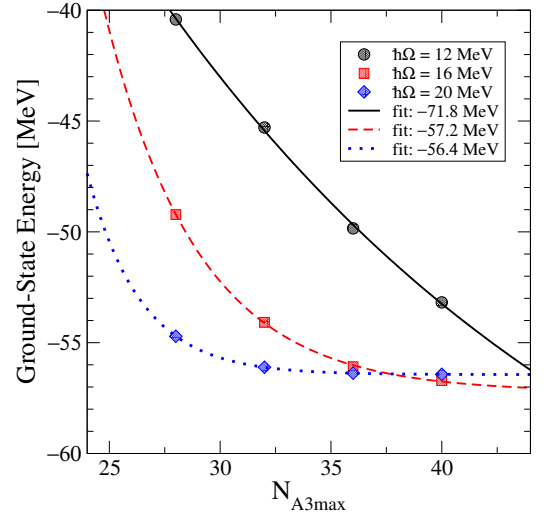

FIG. 4. (color online) Attempted extrapolation in $N_{A3\max}$ at fixed $N_{\max} = 8$ of ^{8}Be ground-state energies from Fig. 3 at several values of $\hbar\Omega$.

fixed $N_{\max} = 8$ (and fixed $N_{A2\max} = 300$) calculations of the ^{8}Be ground state of the same initial NNN interaction evolved in different three-body basis sizes, for a range of $\hbar\Omega$. All results are for $\lambda = 1.5\,\text{fm}^{-1}$. It is evident that $\hbar\Omega = 12$ MeV is far from converged even at the largest value of $N_{A3\max}$ available. Note that we do not expect the different $\hbar\Omega$ calculations in this figure to have the same energy as $N_{A3\max} \to \infty$, because $N_{\max} = 8$ is still unconverged in the many-body system. However, for each individual $\hbar\Omega$ we need convergence for the largest $N_{A3\max}$, as observed for $\hbar\Omega = 20$ MeV. We also note that an exponential model for the convergence in $N_{A3\max}$ does not work, as shown in Fig. 4. For $\hbar\Omega = 20$ MeV we

observe good convergence at $N_{\text{A3max}} = 40$. However, the quality of the exponential fits in Fig. 4 deteriorates as $\hbar\Omega$ decreases below $20\,\text{MeV}$. We conclude that simple exponential extrapolation in N_{A3max} is not an option for $\hbar\Omega = 16\,\text{MeV}$ and below. In particular, while $\hbar\Omega = 16\,\text{MeV}$ is close to converged for ^8Be, this may be less true for larger nuclei, so we will (perhaps conservatively) only consider $\hbar\Omega \geq 18\,\text{MeV}$ to be reliable in the following.

B. Convergence with model space size N_{max}

In Figs. 5 through 13, we show detailed results for the ground-state energy for each of the calculations of Table II as a function of $\hbar\Omega$ for three representative nuclei (^7Li, ^{10}B, and ^{12}C) and basis sizes N_{max} from 2 to 8 (and 10 for some NN-only cases). Panels from left to right show results for decreasing SRG λ. In all panels the symbols connected by dashed lines denote the *ab initio* calculated points at a single N_{max}, while the solid lines are exponential extrapolations at each individual $\hbar\Omega$ based on "Extrapolation B" from Ref. [1]. Extrapolations are given for $N_{\text{max}} = 2\text{–}6$ and $N_{\text{max}} = 4\text{–}8$, with error bars in the latter determined by the difference from the central prediction of the former. For ^7Li and ^{10}B NN-only calculations, there are also extrapolations for $N_{\text{max}} = 6\text{–}10$ with error bars based on $N_{\text{max}} = 4\text{–}8$; see Fig. 5 of Ref. [33] for ^{12}C for results up to $N_{\text{max}} = 10$ with the same NN-only interactions, but without the Coulomb interaction. These figures display the systematics of NCFC convergence of SRG-evolved interactions with and without three-body forces.

Here, we make various summary observations based on these figures (with further discussion of extrapolations in the next section):

- For all calculations, the rate of convergence with basis size N_{max} is greatly accelerated with decreasing λ for $\hbar\Omega$ near the variational minimum. The addition of NNN interactions does not affect the rate substantially. The dependence on $\hbar\Omega$ at low λ is very flat for higher N_{max}.

- In almost all cases, the location of the variational minimum in $\hbar\Omega$ for a given N_{max} shifts to smaller $\hbar\Omega$ as λ decreases. This is expected because the minimum is where the ultraviolet (UV) and infrared (IR) corrections are roughly equal [34]. (See Fig. 17 and the accompanying discussion below.) The contribution from high momentum components of the interactions to low-energy states decreases as λ decreases, so lower λ Hamiltonians are less sensitive to the UV reach in momentum of a truncated HO basis. In other words, the more evolved Hamiltonian is less sensitive to the UV cutoff intrinsic to the HO basis and thus the interplay between UV cutoff and IR distortion is shifted. This results in a systematic shift of the optimal $\hbar\Omega$ to lower values as the Hamiltonian is evolved.

- The location of the minima for NN+NNN-induced calculations are systematically lower in $\hbar\Omega$ than for the corresponding NN+NNN interaction calculations. This is consistent with the induced NNN interaction being softer than the initial NNN interaction. The significance of high momentum components in the initial NNN interaction were already evident above where we saw that they are not as well converged in the $A = 3$ space used for evolution and require larger $\hbar\Omega$. Furthermore, with NN+NNN-induced interactions, the nuclei are systematically less bound than with the NN+NNN interaction, so the wavefunctions will have longer-range exponential tails; as a consequence, the corresponding wavefunction is better represented with a lower $\hbar\Omega$ for NN+NNN-induced calculations than for NN+NNN calculations.

- Results for $\lambda = 1.5\,\text{fm}^{-1}$ and $1.0\,\text{fm}^{-1}$ are sufficiently converged that extrapolations in the non-gray regions (gray shadowing signifies the unreliable region of $\hbar\Omega$ discussed above) are the same for different $\hbar\Omega$ within the (small) error bars. Near the minima in this λ range extrapolation is largely superfluous. In cases including initial or induced NNN interactions, the minimum is sometimes in the gray region. However, in such cases the convergence for larger $\hbar\Omega$ is well advanced and the individual $\hbar\Omega$ extrapolations are consistent with each other.

- Extrapolated results for $\lambda = 2.5\,\text{fm}^{-1}$ (and to some degree for $\lambda = 2.0\,\text{fm}^{-1}$) appear to depend systematically on $\hbar\Omega$. Although it has generally been considered most reliable to extrapolate using energies for $\hbar\Omega$ near the variational minimum, selected results in $N_{\text{max}} = 10$ spaces (e.g., for ^{10}B NN-only) suggest that the extrapolations from 4,6,8 are overbound near the minimum for larger λ (and 2,4,6 even more so), so that estimates from larger $\hbar\Omega$ are more robust. This may be related to the fact that the location of the variational minimum is shifting to larger values of $\hbar\Omega$ as N_{max} increases. In general, our $\lambda \geq 2.2\,\text{fm}^{-1}$ extrapolations for these nuclei have error bars too large to allow useful quantitative conclusions about λ dependence.

- In Figs. 11, 12, and 13, the $\lambda = 2\,\text{fm}^{-1}$ results for ^{12}C at $\hbar\Omega = 20\,\text{MeV}$ include a horizontal line marking the best extrapolated value (with error bar) from the IT-NCSM calculations of Roth et al [18]. The $N_{\text{max}} \leq 6$ values are relatively consistent with the extrapolated IT-NCSM results, but beginning with the extrapolated NCFC results that include the $N_{\text{max}} = 8$ points, we appear to predict somewhat more binding than the IT-NCSM extrapolated result, though our uncertainties are large enough that a definitive conclusion is elusive. Note, however, that the prescription for the N_{A3max} truncation is slightly different in Ref. [18] than what
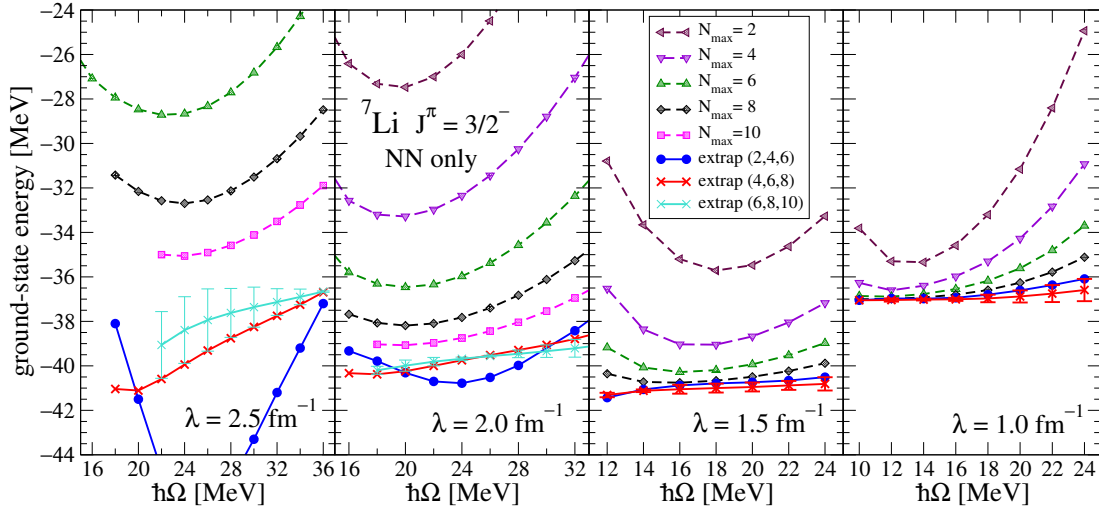
FIG. 5. (color online) Ground-state energy of ^{7}Li for NN-only evolved Hamiltonians at $\lambda = 2.5$, 2.0, 1.5, and $1.0\,\mathrm{fm}^{-1}$, plus extrapolations based on "Extrapolation B" from Ref. [1]. See text for further details.
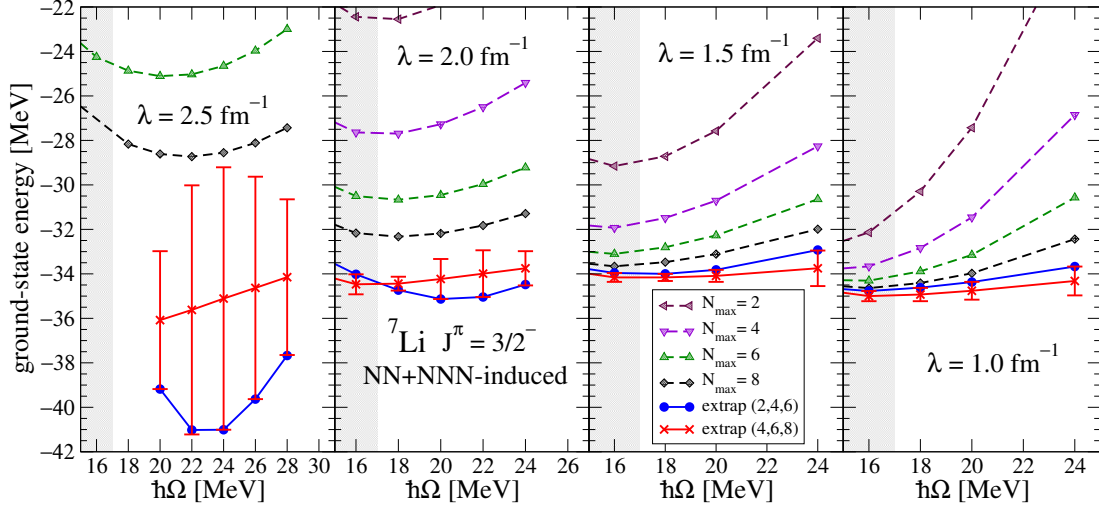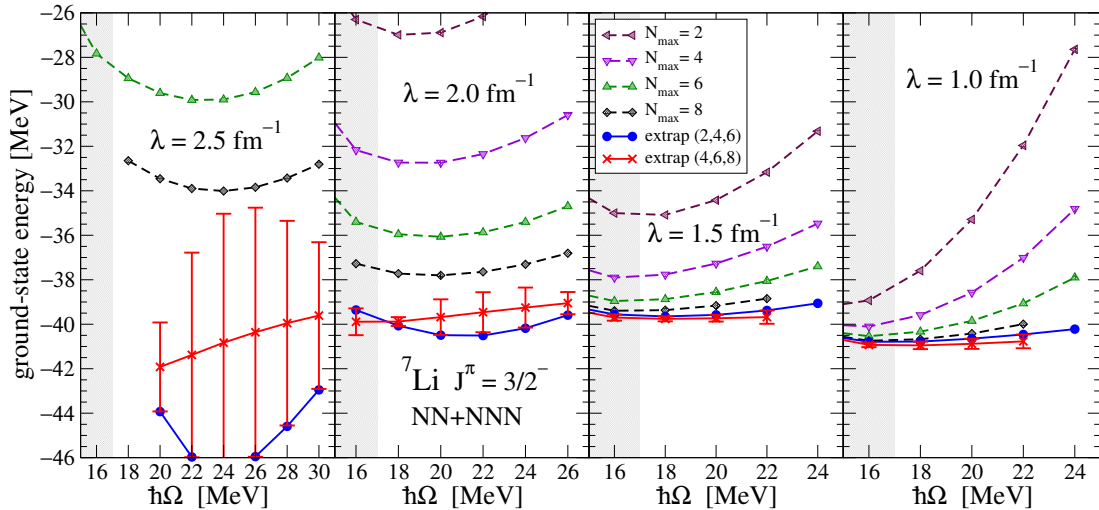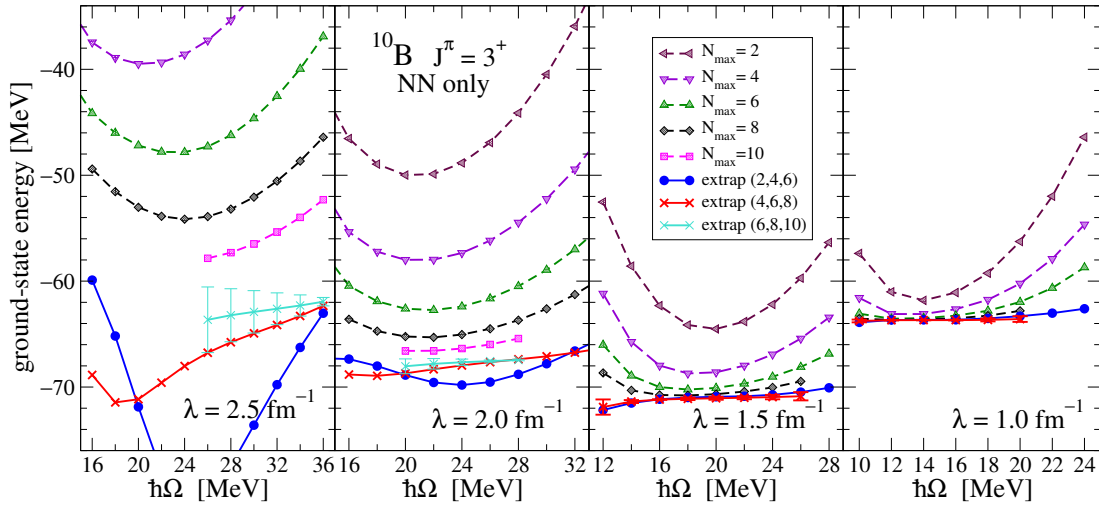

FIG. 6. (color online) Ground-state energy of ^{7}Li for NN+NNN-induced evolved Hamiltonians at $\lambda = 2.5$, 2.0, 1.5, and $1.0\,\mathrm{fm}^{-1}$, plus extrapolations based on "Extrapolation B" from Ref. [1]. The gray shadowing signifies an unreliable region; see text for further details.

FIG. 7. (color online) Ground-state energy of ^{7}Li for NN+NNN evolved Hamiltonians at $\lambda = 2.5$, 2.0, 1.5, and $1.0\,\mathrm{fm}^{-1}$, plus extrapolations based on "Extrapolation B" from Ref. [1]. The gray shadowing signifies an unreliable region; see text for further details.

FIG. 8. (color online) Ground-state energy of ^{10}B for NN-only evolved Hamiltonians at $\lambda = 2.5, 2.0, 1.5,$ and $1.0\,\mathrm{fm}^{-1}$, plus extrapolations based on "Extrapolation B" from Ref. [1]. See text for further details.
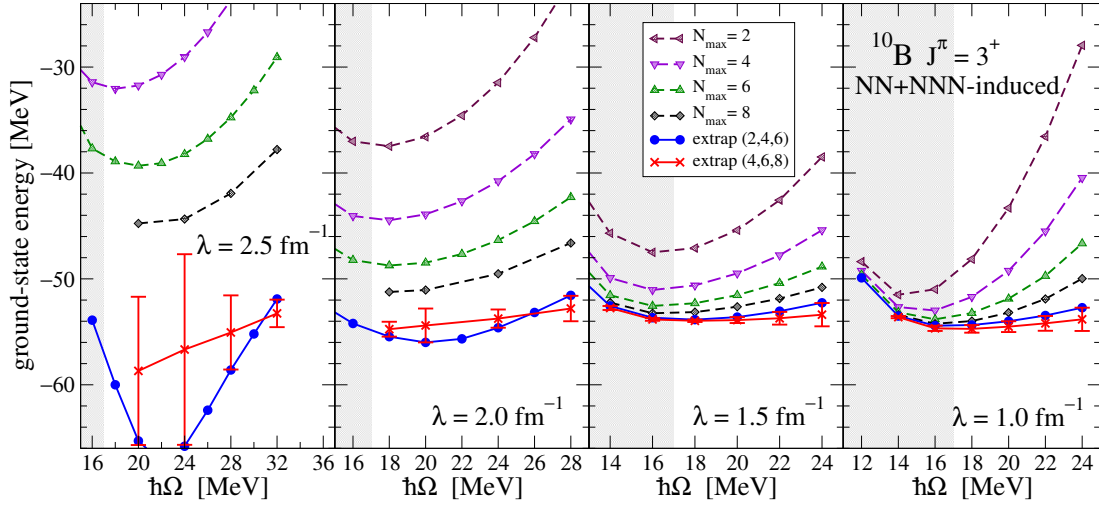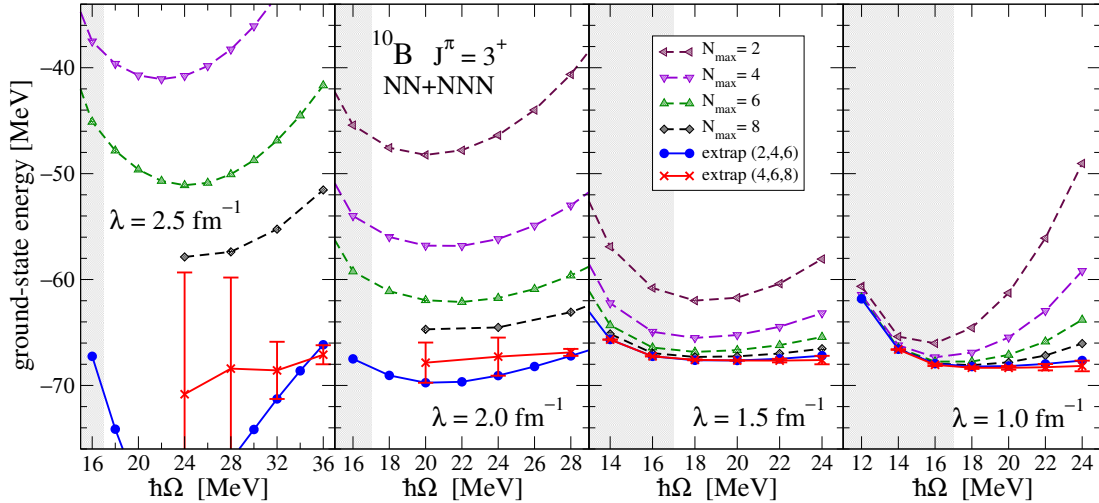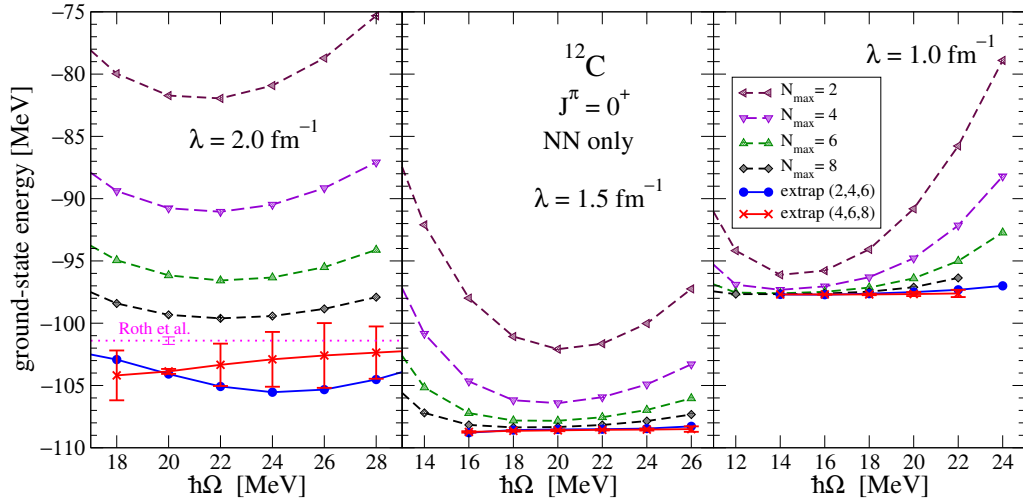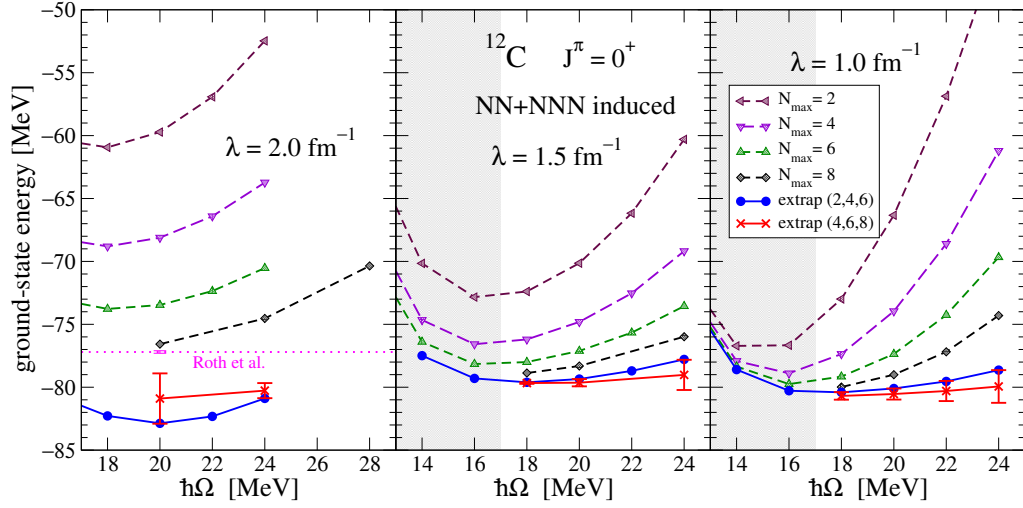

FIG. 9. (color online) Ground-state energy of ^{10}B for NN+NNN-induced Hamiltonians evolved to $\lambda = 2.5, 2.0, 1.5,$ and $1.0\,\mathrm{fm}^{-1}$, plus extrapolations based on "Extrapolation B" from Ref. [1]. The gray shadowing signifies an unreliable region; see text for further details.

FIG. 10. (color online) Ground-state energy of ^{10}B for NN+NNN evolved Hamiltonians at $\lambda = 2.5, 2.0, 1.5,$ and $1.0\,\mathrm{fm}^{-1}$, plus extrapolations based on "Extrapolation B" from Ref. [1]. The gray shadowing signifies an unreliable region; see text for further details.
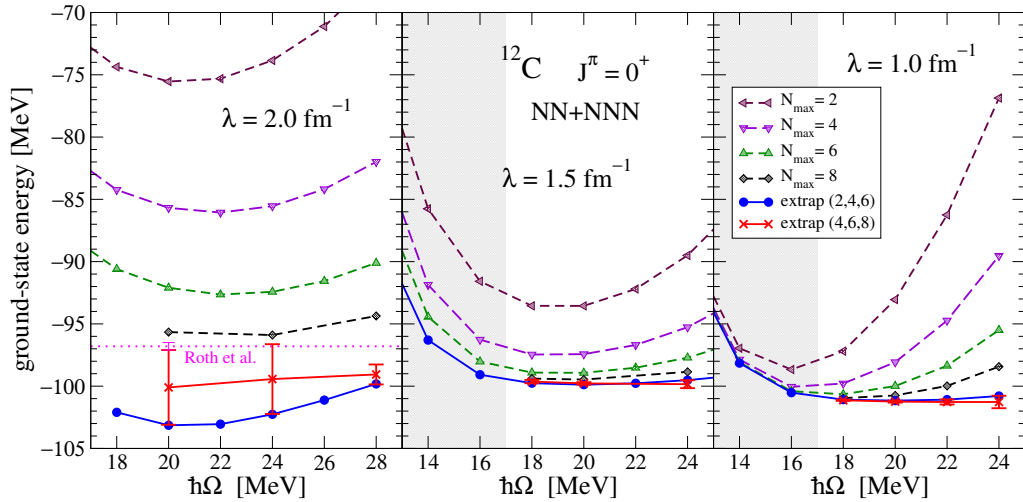
FIG. 11. (color online) Ground-state energy of ^{12}C for NN-only evolved Hamiltonians at $\lambda = 2.0$, 1.5, and 1.0 fm^{-1}, plus extrapolations based on "Extrapolation B" from Ref. [1]. See text for further details.

FIG. 12. (color online) Ground-state energy of ^{12}C for NN+NNN-induced Hamiltonians evolved to $\lambda = 2.0$, 1.5, and 1.0 fm^{-1}, plus extrapolations based on "Extrapolation B" from Ref. [1]. The gray shadowing signifies an unreliable region; see text for further details.

FIG. 13. (color online) Ground-state energy of ^{12}C for NN+NNN evolved Hamiltonians at $\lambda = 2.0$, 1.5, and 1.0 fm^{-1}, plus extrapolations based on "Extrapolation B" from Ref. [1]. The gray shadowing signifies an unreliable region; see text for further details.

we use here. Both in Ref. [18] and in our calculations use $N_{\mathrm{A3max}} = 40$ for the leading, $J = \frac{1}{2}$, 3NF contributions, but we use different cutoffs for the higher-J terms. A detailed analysis of the effect of importance truncation for this particular case is in progress [37].

- It is evident by comparing extrapolated values for NN-only to the NN+NNN calculations that the λ dependence of the extrapolated energies is significantly reduced by including 3NFs. This is summarized in the figures discussed in Section IV.

Overall, the convergence patterns with N_{max} and $\hbar\Omega$ previously observed as a consequence of NN-only SRG evolution [14] are still present when 3NF contributions are included.

C. Comparison of extrapolation methods

The extrapolations in Figs. 5 through 13 are a series of individual extrapolations using Eq. (3), each for a fixed value of $\hbar\Omega$. As noted earlier, the plotted error bars for each $\hbar\Omega$ are determined by comparison of each individual $N_{\mathrm{max}} = 4$–8 extrapolation to that obtained from $N_{\mathrm{max}} = 2$–6. The resulting set of predictions can then be analyzed to obtain a predicted energy and overall error bar [1]. We consider two criteria for determining a best "Extrapolation B" result for E_∞ and the corresponding error bar:

- the result at the $\hbar\Omega$ value for which the amount of extrapolation is minimal (i.e. the point where $E(N_{\mathrm{max}}) - E_\infty$ is minimal);

- the result at the $\hbar\Omega$ value for which the numerical error estimate is minimal.

In both cases, we restrict the best "Extrapolation B" to $\hbar\Omega$ values at or above the variational minimum at the highest N_{max} employed in the extrapolation. For the error estimates we use the average of the error bars in a region of 8 MeV around this best $\hbar\Omega$ value. This initial error estimate is enlarged as necessary in order to get consistent results, such that the central values are within the error estimate in the entire 8 MeV range.

Note that below $\lambda = 1.5\,\mathrm{fm}^{-1}$ with 3NFs, we cannot apply either of these criteria, because we are only using results for $\hbar\Omega \geq 18\,\mathrm{MeV}$, and the variational minimum is typically at or below $\hbar\Omega = 18\,\mathrm{MeV}$ for the lowest λ values; however, for these values of λ the results are quite close to convergence, and we base our error estimate on the results for $18 \leq \hbar\Omega \leq 24\,\mathrm{MeV}$. Above $\lambda = 1.8\,\mathrm{fm}^{-1}$, the two criteria give (slightly) different results, but generally with overlapping extrapolation error estimates.

The convergence pattern and extrapolations of the NN-only data up through $N_{\mathrm{max}} = 10$ (see Figs. 5 and 8, as well as Fig. 5 of Ref. [33]), suggest that for $\lambda = 2.5\,\mathrm{fm}^{-1}$

the $\hbar\Omega$ value that minimizes the numerical error estimate, $\hbar\Omega \simeq 36\,\mathrm{MeV}$, is more reliable for the extrapolation (at least at this λ value) than the $\hbar\Omega$ value that minimizes $E(N_{\mathrm{max}}) - E_\infty$. (With the nonlocal NN interaction JISP16, for which this extrapolation has been used extensively [1, 3, 38] these two criteria rarely lead to significant differences.)

An alternative approach is to use a constrained optimization that uses all (or a specified subset) of $\hbar\Omega$ data, requiring the same extrapolated energy E_∞ in Eq. (3) for every $\hbar\Omega$, such as "Extrapolation A" of Ref. [1]. Here, we use basically the same procedure for the constrained optimization, using four subsequent N_{max} values and five $\hbar\Omega$ values for each constrained fit, with the same weights and error estimate as in Ref. [1]. (For the current calculations five $\hbar\Omega$ values span an 8 MeV range of $\hbar\Omega$, whereas in Ref. [1] it spans a 10 MeV range.) Again, with 3NFs this procedure cannot be applied below $\lambda = 1.5\,\mathrm{fm}^{-1}$, but the results are close to convergence for these cases, and therefore less sensitive to the details of the extrapolation. For $1.5\,\mathrm{fm}^{-1} \geq \lambda \geq 2\,\mathrm{fm}^{-1}$ the results from "Extrapolation A" are consistent with those from "Extrapolation B", but for $\lambda > 2\,\mathrm{fm}^{-1}$ the procedure of Ref. [1] for "Extrapolation A", modified as described above, leads to results that show a systematic deficiency at $N_{\mathrm{max}} = 10$.
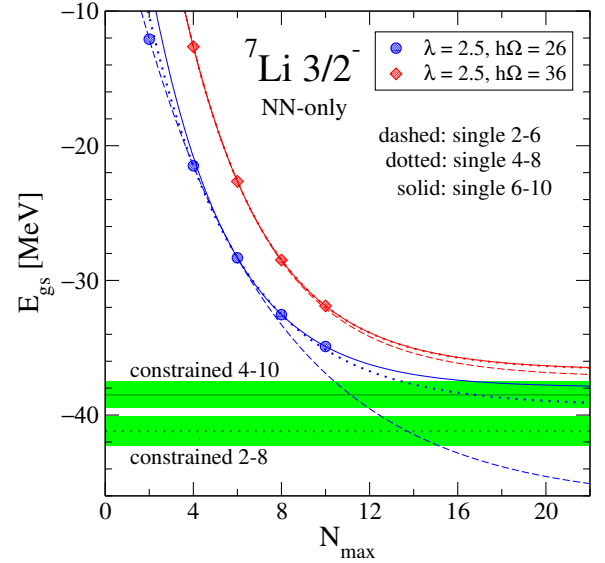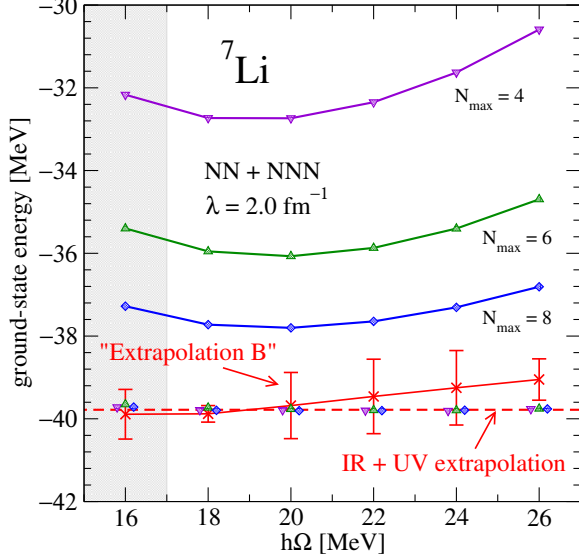

FIG. 14. (color online) Ground-state energy extrapolations of ^{7}Li as a function of N_{max} with an N^{3}LO NN interaction [21] evolved to $\lambda = 2.5\,\mathrm{fm}^{-1}$. The symbols are the calculated points. The curves show single extrapolations using Eq. (3) with $N_{\mathrm{max}} = 2$–6 (dashed), 4–8 (dotted) and 6–10 (solid) at (blue) $\hbar\Omega = 26\,\mathrm{MeV}$ which minimize the amount of extrapolation and at (red) $\hbar\Omega = 36\,\mathrm{MeV}$ which minimize the numerical error estimate. The horizontal dotted and solid lines, with the band indicating the associated error bars, are the result from a constrained fit following the procedure of Ref. [1] for five $\hbar\Omega$ values from 22 to 30 MeV.

Figure 14 shows a comparison of the single and the constrained extrapolation schemes for $\lambda = 2.5\,\mathrm{fm}^{-1}$. In

this example we use ^{7}Li with NN-only calculations up to $N_{\max} = 10$. The variational minimum is at 24 MeV, so we use five $\hbar\Omega$ values from 22 MeV to 30 MeV, and four $N_{\max}$ values for each $\hbar\Omega$ for the each of the constrained fits. Figure 14 shows clearly that this procedure with the $N_{\max} = 2$ to 8 results leads to an overestimate of the binding energy and an underestimate of the extrapolation uncertainty. In Fig. 14, we can also see why this procedure leads to erroneous results: near the variational minimum the convergence is not a simple exponential for this value of λ, as is evident from the single $\hbar\Omega$ fits (blue curves).

FIG. 15. (color online) Ground-state energy of ^{7}Li for NN+NNN evolved Hamiltonians at $\lambda = 2.0\,\mathrm{fm}^{-1}$, plus extrapolations based on "Extrapolation B" from Ref. [1] (solid line and points with error bars) and on the combined IR/UV correction formula Eq. (5) that yields E_∞ (dashed line) and individual corrections for each $\hbar\Omega$ and $N_{\max}$ combination (points near the dashed line) based on the single set of best-fit parameters. The gray shadowing signifies an unreliable region (see text).

The alternative EFT-motivated approach described in Sec. II C is complementary to the schemes used in Figs. 5–14. A sample application of Eq. (5), which includes both UV and IR corrections to the energy at each $N_{\max}$ and $\hbar\Omega$, is shown in Fig. 15 for the NN+NNN calculation of the ^{7}Li ground state. In this example, the fifteen points with $\hbar\Omega \geq 18\,\mathrm{MeV}$ and $N_{\max}$ from 4 to 8 are inputs to a simultaneous fit of the five parameters of $E(\Lambda_{UV}, L)$ with Λ_{UV} and L given as functions of $\hbar\Omega$ and $N_{\max}$ (see Sec. II C for the formulas, recalling that we will use $N = N_{\max} + 3$ for p-shell nuclei). The result for E_∞ (dashed line) is consistent with the individual "Extrapolation B" results (from Fig. 7) and the overall result is within the error bars of that scheme. An error analysis procedure for the IR/UV correction model is not yet available, which limits its utility for the present analysis, but the goodness-of-fit can be assessed by the (very
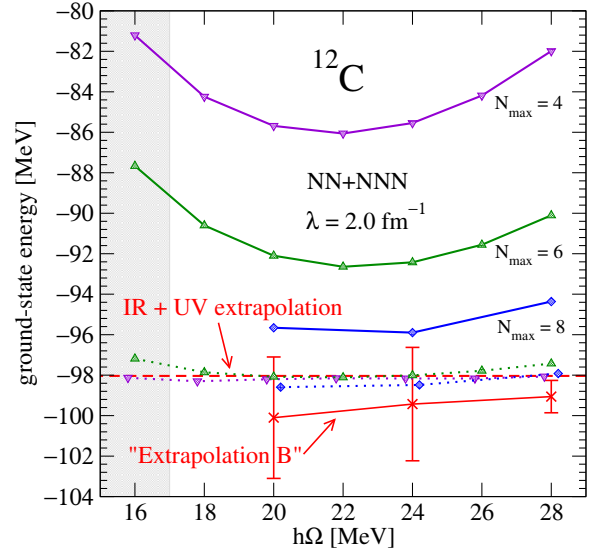

FIG. 16. (color online) Ground-state energy of ^{12}C for the NN+NNN evolved Hamiltonians at $\lambda = 2.0\,\mathrm{fm}^{-1}$, plus extrapolations based on "Extrapolation B" from Ref. [1] (solid line and points with error bars) and on the combined IR/UV correction formula Eq. (5) that yields E_∞ (dashed line) and individual corrections for each $\hbar\Omega$ and $N_{\max}$ combination (points near the dashed line) based on the single set of best-fit parameters. The gray shadowing signifies an unreliable region (see text).

small) spread of corrected points about the dashed line. Corrected points represent the use of the best fit parameters with Eq. (5) (except E_∞) to extend each finite basis result to infinite $N_{\max}$ at fixed $\hbar\Omega$. Note also the predictions for the $\hbar\Omega = 16\,\mathrm{MeV}$ points, although those data points were not included in the fit.

A second extrapolation based on the IR/UV correction model is shown in Fig. 16, where the spread of corrections indicates a still good but less-than-ideal fit for the NN+NNN calculation of the ^{12}C ground state. Note that the largest deviations of the corrected results from the fit E_∞ occur for two of the three highest $N_{\max}$ points. The implication is that the true E_∞ should be slightly more negative, which is also the conclusion from comparing with the "Extrapolation B" analysis. Note, however, that although we used the same total number of points for this IR/UV extrapolation, we have only three $N_{\max} = 8$ points (see Fig. 13, compared to five of the fifteen points that we used for Fig. 15.

In general, a good fit requires the UV and IR functional forms to be adequate models for smaller $N_{\max}$ values (with increasing $N_{\max}$ there is decreasing sensitivity while the computational cost is increasing dramatically). Much remains to be explored for heavier nuclei but detailed investigation of two-particle models and the deuteron suggest that the forms in Eq. (5) can be improved and that the predictions can be sensitive to optimizing the choice of expressions for L and Λ_{UV} [36] (e.g., using $N_{\max} + 3/2 + 2$ rather than $N_{\max} + 3/2$ for

two-body systems). We are also not yet able to take advantage of the theoretical prediction that k_∞ should be related to the nucleon separation energy and the empirical observation that B_1 is found to be numerically close to λ.

The two examples considered so far are for $\lambda = 2\,\mathrm{fm}^{-1}$. For $\lambda \leq 1.5\,\mathrm{fm}^{-1}$, the new extrapolation method using data up to $N_{\max} = 8$ gives predictions for the $N_{\max} = \infty$ energies consistent with the other extrapolation schemes. As already noted, there are some systematic differences for $\lambda = 2\,\mathrm{fm}^{-1}$, but they are within the "Extrapolation B" uncertainties. For larger λ these differences grow, but it is not possible at present to determine which approach is superior.
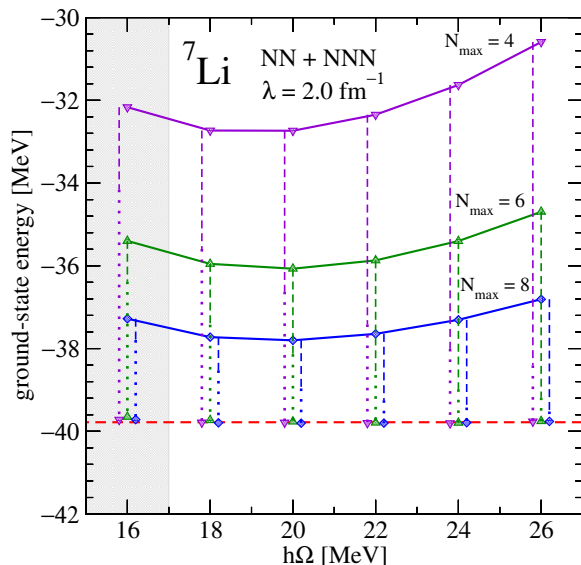

FIG. 17. (color online) Ground-state energy of ^{7}Li for the NN+NNN evolved Hamiltonians at $\lambda = 2.0\,\mathrm{fm}^{-1}$, with IR (vertical dashed) and UV (vertical dotted) corrections from Eq. (5) that add to predicted E_∞ values (points near the horizontal dashed line, which is the global E_∞). The gray shadowing signifies an unreliable region (see text).

It is instructive after making a global fit to decompose each correction for a given $\hbar\Omega$ and $N_{\max}$ into the individual IR and UV contributions. This is done in Fig. 17 for the ^{7}Li fit of Fig. 15. This figure verifies our prior claim that IR and UV corrections are roughly equal at the variational minima, while the IR(UV) correction rapidly dominates when we move to the right(left) of a minimum. If there are enough $(\hbar\Omega, N_{\max})$ points calculated where one of the two corrections is numerically insignificant, a simpler extrapolation with only three fit parameters is possible. An example of an IR-only fit is given for the NN-only calculation of ^{10}B at $\lambda = 2\,\mathrm{fm}^{-1}$ is given in Fig. 18. Such IR-only fits are not possible for the calculations here including NNN because we do not have enough points sufficiently removed from the minimum in $\hbar\Omega$.
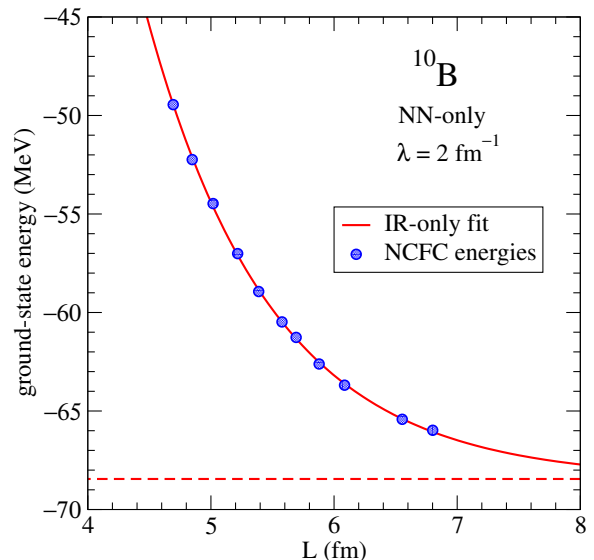

FIG. 18. (color online) Ground-state energy of ^{10}B for the NN-only evolved Hamiltonians at $\lambda = 2.0\,\mathrm{fm}^{-1}$ for $N_{\max} = 4$–8 and $\hbar\Omega = 28$–$32\,\mathrm{MeV}$ plus $N_{\max} = 10$ and $\hbar\Omega = 26, 28\,\mathrm{MeV}$ with an IR-only fit using Eq. (6). The fit value of E_∞ is the dashed line.

The points in Fig. 18 were chosen to the right of the variational minimum (see Fig. 8), where a fit to Eq. (5) implies that the UV correction to these points is much smaller than the IR correction. The observation that the points with different $\hbar\Omega$ and $N_{\max}$ values all lie on the same curve verifies that L is the correct variable. We note similar demonstrations for ^{6}He results in Fig. 4 of Ref. [34] with the same NN-only interaction and in Fig. 11 of Ref. [35] using a different NN interaction. The fit to

$$E(L) \approx E_\infty + B_2 e^{-2k_\infty L}\;, \qquad (6)$$

for the energies shown in Fig. 18 is very good. However, the prediction for E_∞ is about 0.6 to 1 MeV more bound than that from the "Extrapolation B" analysis.

It would be premature to draw robust conclusions on the relative efficacy of the extrapolation schemes used here. In particular, further comparisons are needed where large $N_{\max}$ results are available to check small $N_{\max}$ extrapolations. However, for our present purposes it is sufficient that the results of the different schemes are consistent with each other to within the assessed uncertainties currently available. For the remainder of this work, we will use extrapolation procedures based on Eq. (3).

IV. EVOLUTION

A. Running of ground-state energies

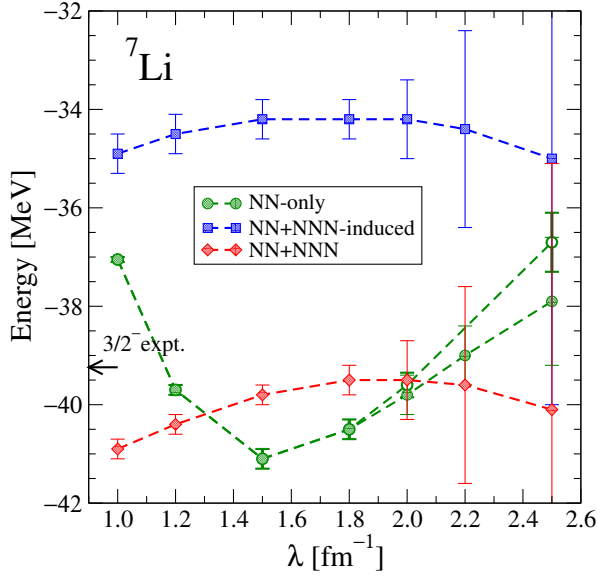In Figs. 19–22, we show the dependence on λ of the ground-state energy in ^{7}Li, ^{8}Be ^{10}B, and ^{12}C using our

FIG. 19. (color online) Extrapolated ground-state energy of ^{7}Li as a function of λ for each SRG calculation. The initial interaction was N^{3}LO NN [21] included up to $N_{\mathrm{A2max}} = 300$ and N^{2}LO NNN [29, 39] up to $N_{\mathrm{A3max}} = 40$. The dashed curves connect data points and error bars obtained using the extrapolations described in the text. The small black arrow on the left shows the experimental value.
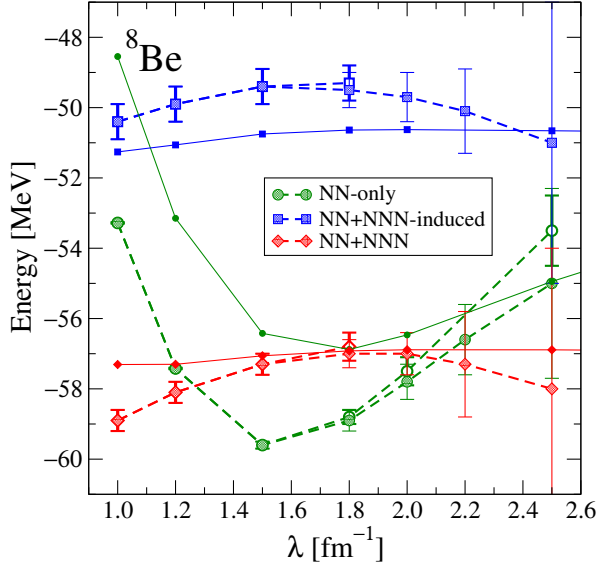

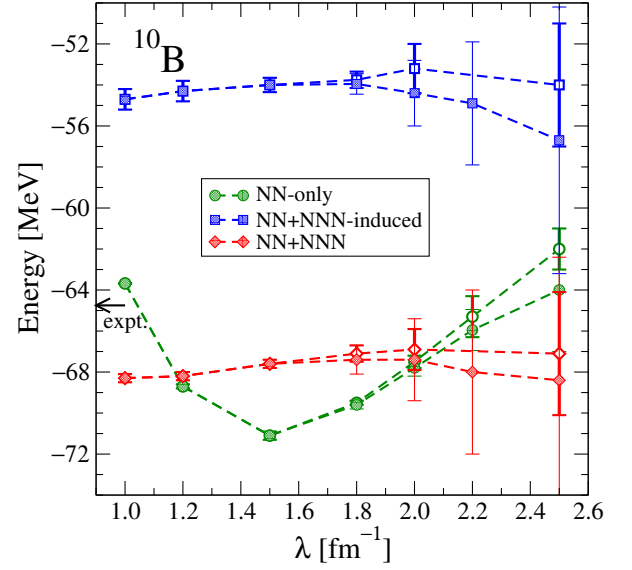FIG. 21. (color online) Same as Fig. 19 but for the ^{10}B ground state. The small black arrow on the left shows the experimental value.

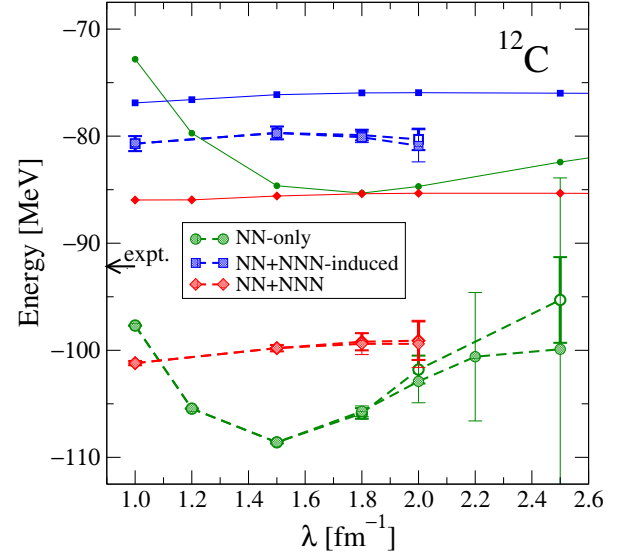FIG. 20. (color online) Same as Fig. 19 but for the ^{8}Be ground state, as well as twice the ^{4}He ground state energy (solid curves).

FIG. 22. (color online) Same as Fig. 19 but for the ^{12}C ground state, as well as three times the ^{4}He ground state energy (solid curves).

best estimate for infinite-basis space results based on "Extrapolation B" described in the previous section. For $\lambda < 1.5 \, \mathrm{fm}^{-1}$ there is good convergence with small error bars, although the numerical accuracy of the extrapolation with 3NFs is limited by the N_{A3max} cutoff. For $\lambda > 1.5 \, \mathrm{fm}^{-1}$ the two criteria for selecting the optimal $\hbar\Omega$ lead to (slightly) different results, and their differ-

ence grows with λ; the shaded symbols in Figs. 19–22 correspond to using the $\hbar\Omega$ value that minimizes $E(N_{\max}) - E_\infty$, whereas the open symbols correspond to using the $\hbar\Omega$ value that minimizes the numerical error estimate. For many cases we currently do not have data available to perform extrapolations at or near the $\hbar\Omega$ value that would minimize the numerical error estimate.

Nevertheless, we see in these figures that for λ between 1.0 and 2.0 fm^{-1} the general pattern is the same as that observed for ^{4}He in Fig. 1. We expect that the NN-only (green circles) start for $\lambda = \infty$ at an (underbound) en-

ergy but the larger λ's required to verify this are not sufficiently converged here. However, the characteristic dip due to omitted induced NNN forces is clear in each of the nuclei. Including the induced NNN matrix elements (blue squares) significantly reduces but does not eliminate the dependence on λ. (Note that, as observed in Fig. 1, the NN-only curve should be equal to the NN+NNN induced result at large λ, which is plausible from Figs. 19–22 but not verifiable in the present calculations.) The trend of the results with induced NNN interactions is increased binding as λ decreases from 1.8 to 1.0 fm^{-1}, consistent with ^{4}He shown in Fig. 1. The magnitude of the decrease is about 0.7–1.1 MeV, without a systematic dependence on the nucleus. When initial NNN interactions are included (red diamonds), the qualitative dependence on λ over this same range is similar, but the magnitude of the decrease is systematically larger by roughly 1 MeV or a factor of two (less in ^{10}B). The downward shift in ground-state energies takes them below the experimental values for the four nuclei of Figs. 19–22. The additional binding provided by the initial 3NF increases from less than one MeV per nucleon in ^{7}Li to more than 1.5 MeV per nucleon in ^{12}C, almost independent of λ for λ between 1.0 and 2.0 fm^{-1}.

The shape of an evolution curve (as in Figs. 19–22) is determined by the interplay of short- and long-range effects in a given A-body sector. This has been demonstrated explicitly in Ref. [28] for a model but needs to be more systematically verified in realistic systems. For a given Hamiltonian (i.e. fixed initial interactions and fixed truncation of the evolution equations at the 2-body or at the 3-body level) we observe close similarity between the various nuclear ground-state evolution curves presented here. Focusing on the range in λ where the error bars are smaller ($\lambda = 1.0$–1.8 fm^{-1}), the energy variations for the NN-only calculations are reduced by a factor of 4–5 for the NN+NNN calculations (and more for NN+NNN-induced). Thus the induced NNN interaction acts to (almost) restore λ-independence in this region, with the residual variation attributed to four-body (and higher) forces.

This suggests that the induced NNN interaction, as in the ^{4}He case, is the leading correction to the NN-only results arising from SRG evolution. Moreover, the similar shapes of the evolution curves through the range of A is also consistent with the preservation of hierarchical induced many-body forces; that is, we expect that the induced four-body forces will provide a residual contribution smaller than the induced NNN interaction. This conclusion is also consistent with previous analysis of expectation values for components of the evolved interaction [16].

The net induced 4NF contribution in ^{4}He was found to be a few hundred keV at $\lambda = 1$ fm^{-1} (see Fig. 1). In Figs. 19–22 the effect of omitted induced four-body (and higher) forces at lower λ (judging solely from the vertical range of each curve) is at least of order 1 to 2 MeV, depending on whether initial 3NFs are included. This is

still small enough that for light nuclei it may be possible to exploit very highly evolved Hamiltonians, especially if a simple approximation for the 4NF contribution can be found. Alternatively, incorporating the induced 4NF contribution explicitly may become computationally feasible in the near future. A quantitative understanding of the magnitude and scaling of (assumed) induced 4NFs with λ and with A is still lacking. This has become an important issue in light of the growing overbinding with larger A observed by Roth et al. when an initial 3NF is included (unless the 3NF cutoff is significantly reduced with respect to the NN cutoff) [18].

In Fig. 20, we also show the evolution curves for two α-particles, noting that the λ-dependence is significantly stronger for ^{8}Be than for two α-particles. With the NN-only interaction, ^{8}Be is actually bound for $\lambda \leq 2$ fm^{-1}, but once the induced 3NF is included, it appears to be unbound by about 1 MeV. With the initial 3NFs we find that ^{8}Be is bound for $\lambda \leq 1.5$ fm^{-1}, but for larger values of λ we cannot draw a firm conclusion. Experimentally, ^{8}Be is unbound by about 0.1 MeV (i.e. the lowest lying narrow resonance is 0.1 MeV above the two-α threshold). In Fig. 22, we also show three times the ground state energy of ^{4}He. With the NN-only potential, ^{12}C is bound by about 20 to 25 MeV relative to three α particles with the same interaction for λ between 1 and 2 fm^{-1}, but once the induced 3NFs are taken into account, it is bound by only about 4 MeV. Once the initial N2LO chiral 3NFs are incorporated, the binding relative to three α's increases to about 14 MeV, and is nearly independent of λ. Experimentally, this energy difference is about 7.5 MeV. We expect that the overbinding by almost a factor of two relative to the three α threshold with the chiral N2LO 3NFs will have important consequences for the low-lying spectrum of ^{12}C, in particular for the Hoyle state.

B. Low-lying excited states

In Figs. 23–25, we show the excitation energies of the lowest excited states in ^{7}Li, ^{8}Be, and ^{10}B as function of $\hbar\Omega$ for different values of λ at fixed $N_{max} = 8$. For ^{7}Li and ^{8}Be, the excitation energy of the first excited state is almost independent of both λ and $\hbar\Omega$, and in good agreement with experiment. This independence suggests that these excitation energies are close to being converged. The second excited state of these nuclei shows a slight dependence on both λ and $\hbar\Omega$. In particular, at larger values of λ the excitation energies show a variation with $\hbar\Omega$ indicating that these excitation energies are not yet converged. However, this variation is significantly less than the estimated extrapolation error in the absolute (ground state) energies for these nuclei. More interesting is that the (albeit small) dependence on λ is significantly larger with initial 3NFs than with induced 3NFs only, as is evident by the smaller spread of the curves in the left panels of Figs. 23 and 24.

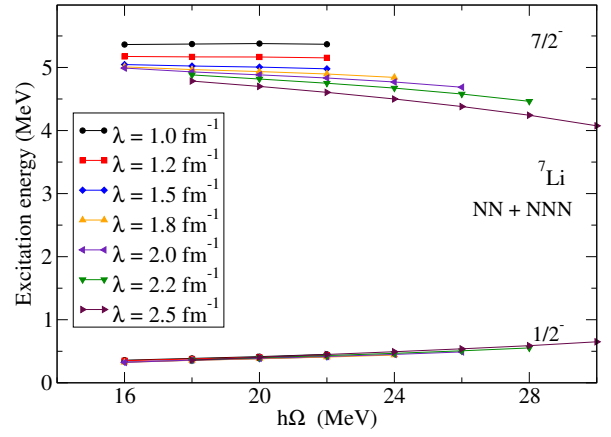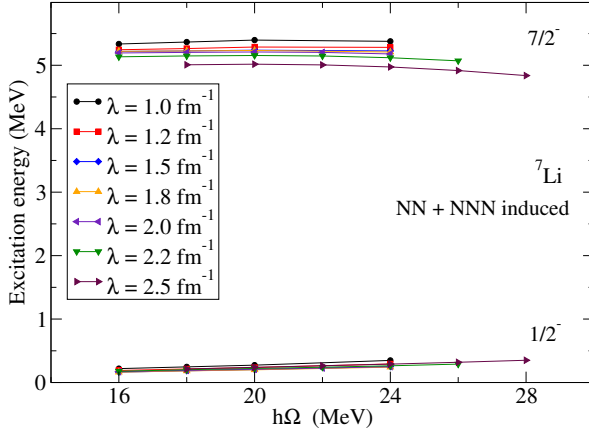In ^{10}B the situation is much more complicated. In

FIG. 23. (color online) Lowest two excited states ^{7}Li as a function of $\hbar\Omega$ for each SRG λ value at $N_{\max} = 8$. The initial interaction was N^{3}LO NN [21] included up to $N_{A2\max} = 300$ and N^{2}LO NNN [29, 39] up to $N_{A3\max} = 40$. The small black arrow on the left shows the experimental value.
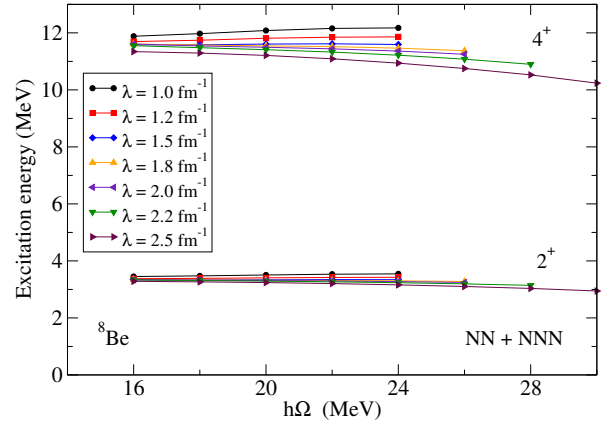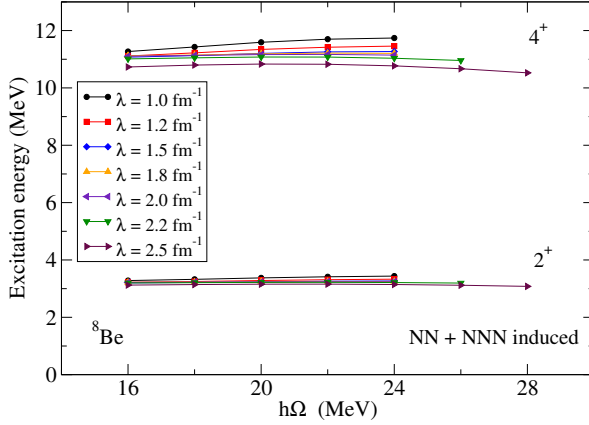

FIG. 24. (color online) Lowest two excited states ^{8}Be as a function of $\hbar\Omega$ for each SRG λ value at $N_{\max} = 8$. The small black arrow on the left shows the experimental value.

Fig. 25, we show the excitation energies of the lowest four excited states of ^{10}B relative to the $(3^+, 0)$ (which is the ground state of ^{10}B): two $(1^+, 0)$ states, a $(2^+, 0)$ state, and a $(0^+, 1)$ state (analog state of the ground state of ^{10}Be and ^{10}C). It is immediately obvious that there is a much larger spread in the excitation energies than for ^{7}Li and ^{8}Be, in particular with initial 3NFs.

With induced 3NFs only, the lowest state is actually a $(1^+, 0)$ state, rather than the $(3^+, 0)$. This state however is rather poorly converged relatively to the $(3^+, 0)$ state, as is evident from the strong $\hbar\Omega$ dependence of its (mostly negative) excitation energy, even for very small values of λ. Furthermore, the second $(1^+, 0)$, as well as the lowest $(2^+, 0)$ and $(0^+, 1)$ states are very close to each other, all with excitation energies between 1 and 2 MeV, and all with a similar weak λ and moderate $\hbar\Omega$ dependence. Experimentally, these three states have excitation energies of 2.154 MeV, 1.740 MeV, and 3.587 MeV respectively. Thus, in the absence of initial 3NFs, the chiral interactions not only predict the wrong ground state for

^{10}B but also a much too dense spectrum for the other low-lying states.

With initial 3NFs the spectrum looks quite different. One of the two $(1^+, 0)$ becomes strongly dependent on λ, whereas the other $(1^+, 0)$ state remains almost independent of λ. In the region of parameter space where these two states are well-separated, they can be distinguished by their quadrupole and magnetic moments. Although the quadrupole moments are not converged, they are clearly different for these two states: one has a small positive quadrupole moment of the order of one e fm^2 or smaller (open symbols in Fig. 25), whereas the other has a negative quadrupole moment around -2 to -3 e fm^2 (solid symbols in Fig. 25). The latter of these two states depends only weakly on λ and $\hbar\Omega$, and appears to be reasonably well converged, whereas the former is very strongly dependent on both λ and $\hbar\Omega$, and is not converged at all. However, for λ from 1.5 fm^{-1} to 2.0 fm^{-1} these two states show significant mixing. (Experimentally, they are separated by about 1.4 MeV.) For com-
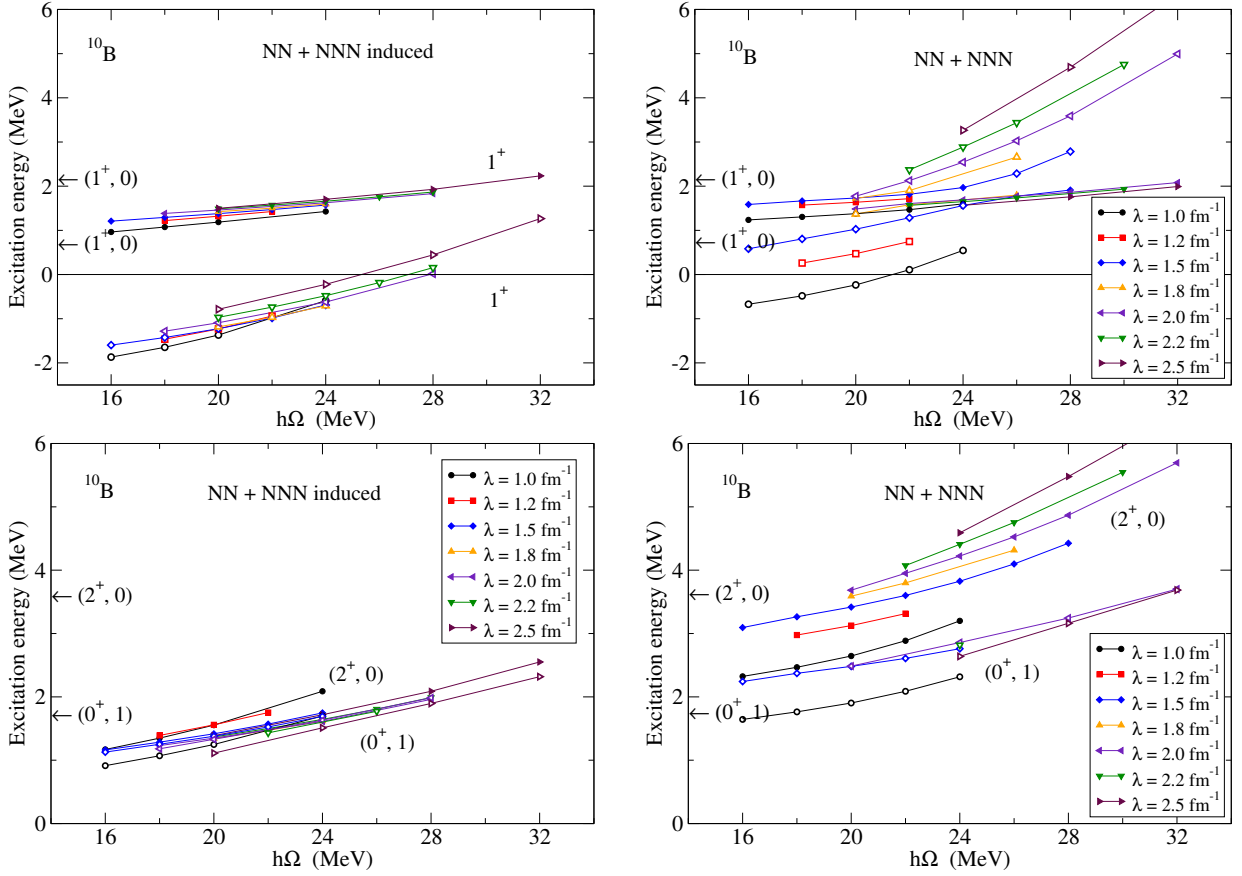
FIG. 25. (color online) Lowest excited states ^{10}B as a function of $\hbar\Omega$ for each SRG λ value at $N_{\max} = 8$. The small black arrows on the left shows the experimental values.

parison, the quadrupole moment of the ground state is about $+7$ to $+8$ e fm^2 with induced 3NFs only, and about $+6$ to $+7$ e fm^2 with initial 3NFs, in reasonable agreement with the experimental value of $+8.472(56)$ e fm^2, given the fact that the quadrupole moments are not yet converged in these basis spaces. It will take a major effort to develop robust extrapolation and error quantification tools for long-range operators, such as quadrupole operators. We therefore defer a detailed consideration of these operators until those tools are developed.

For small values of λ, the slowly converging $(1^+, 0)$ state with a small quadrupole moment actually becomes the lowest state, even with initial 3NFs. It is likely that for this state the induced four-body (and higher-body) interactions, which have been omitted in the present calculations, are important, though without convergence it is hard to draw firm conclusions. It is also possible that the strong λ dependence is caused by the lack of convergence, and that once convergence (i.e. independence of both $N_{\max}$ and $\hbar\Omega$) is reached the results will be much less dependent on λ.

The other excited states shown in Fig. 25, namely the $(0^+, 1)$ (open symbols) and the $(2^+, 0)$ (solid symbols), show a strong dependence on both λ and $\hbar\Omega$ with initial 3NFs. Clearly, these excitation energies are not very well

converged, but nevertheless we can see that the overall effect of the initial 3NFs is to increase their excitation energy and to separate these two states from each other, in qualitative agreement with the data.

A striking difference between Figs. 23 and 24 on the one hand, and Fig. 25 on the other, is the strong λ and $\hbar\Omega$ dependence of the excitation energies in Fig. 25 (with the possible exception of one of the two low-lying $(1^+, 0)$ states) compared to the independence of λ and $\hbar\Omega$ of the excitation energies in Figs. 23 and 24. One possible explanation for this observation is that the excited states in Figs. 23 and 24 can be interpreted as rotational excitations of the ground state [40]. Thus these states have a very similar structure, and are therefore likely to exhibit a similar convergence pattern (i.e. $\hbar\Omega$ dependence) and λ dependence. We also see this in ^{12}C, where the lowest 2^+ and 4^+ states form a rotational band with the ground state [33], but other low-lying states in ^{12}C are much more sensitive to the 3NFs and have a different convergence pattern [37].

Finally, we also calculated the magnetic moments of ^{7}Li, ^{7}Be, and ^{10}B, see Table III. The quoted numerical uncertainty in Table III includes both the dependence on the basis space parameters (i.e. $\hbar\Omega$ and $N_{\max}$ dependence) and the λ dependence. At $N_{\max} = 8$ the magnetic

TABLE III. Magnetic moments for ^{7}Li, ^{7}Be, and ^{10}B with the NN+NNN-induced and NN+NNN interactions.

Nucleus	state	induced	NNN	expt.
^{7}Li	$\frac{3}{2}^-$	3.0(1)	3.0(1)	3.2564
^{7}Li	$\frac{1}{2}^-$	−0.8(1)	−0.8(1)	
^{7}Li	$\frac{7}{2}^-$	3.5(2)	3.2(3)	
^{7}Be	$\frac{3}{2}^-$	−1.15(5)	−1.15(6)	−1.399
^{7}Be	$\frac{1}{2}^-$	1.18(3)	1.22(3)	
^{7}Be	$\frac{7}{2}^-$	0.24–0.56	0.37–1.07	
^{10}B	3^+	1.85(1)	1.83(2)	1.8006
^{10}B	1^+	0.84(2)	0.78–0.85	0.63(12)
^{10}B	1^+	0.35(2)	0.34–0.41	

moments are typically converged to within a few percent, and the influence of the SRG evolution is less than a few percent, except for the $\frac{7}{2}^-$ state of ^{7}Be and the two $(1^+, 0)$ states in ^{10}B. A closer look at the different components contributing to the magnetic moment of the $\frac{7}{2}^-$ state of ^{7}Be shows that the contributions from the neutron intrinsic spin and from the proton angular momentum nearly cancel, leaving the proton intrinsic spin contribution to dominate the magnetic moment, both with and without initial 3NFs. For the two states in ^{10}B, most of the parameter dependence of the magnetic moments for these two states is due to (strong) mixing. In general, adding initial 3NFs to the chiral N3LO NN interaction does not have a significant effect on these magnetic moments.

These magnetic moments are calculated in impulse approximation, using the canonical M1 operator. Of course, we should use a current operator that is consistent with the chiral Hamiltonian that we are using: for the ground state of ^{7}Li and ^{7}Be we might expect, based on Refs [41, 42], a correction due to meson exchange currents of about 10%, in the direction that would bring our results toward agreement with experiment.

V. CONCLUSIONS

We have presented *ab initio* NCFC calculations of energies in the p-shell using SRG-evolved two- and three-nucleon forces. Several different procedures were considered to extrapolate energies to infinite harmonic-oscillator basis size; for the range in the evolution parameter λ we focus on (from 1 to $2\,\mathrm{fm}^{-1}$) they give consistent results within estimated error bars. Error bars above $2\,\mathrm{fm}^{-1}$ grow rapidly and limit what we can quantitatively conclude about λ dependence. As anticipated from results with lighter nuclei, inclusion of induced NNN interaction significantly reduced the λ dependence of ground-state energies compared to NN-only calculations for all nuclei considered. Furthermore, the rapid improvement of convergence with decreasing λ of ground-state and low-lying state energies observed for

NN-only calculations [14] carries over when only induced NNN interactions are included. With initial NNN interactions, ground-state convergence is similarly improved but some excited states show very different behavior, see Fig. 25.

With NN+NNN-induced interactions (but without initial NNN interactions), the net change in total ground-state energy for nuclei in the p-shell was found to be small (and within extrapolation error bars) between $\lambda = 2.0\,\mathrm{fm}^{-1}$ and $\lambda = 1.5\,\mathrm{fm}^{-1}$, but systematically decreases (becomes more bound) as λ decreases to $1.0\,\mathrm{fm}^{-1}$ by about $1\,\mathrm{MeV}$. The A dependence is small. This additional binding can be attributed to four- and higher-body forces, which is of natural size (as implied by EFT power counting) despite the extreme degree of softening. While this might appear to be a narrow range in λ, we emphasize that there is significant evolution (e.g., note that the natural SRG evolution variable $s = 1/\lambda^4$ increases by a factor of 16 as λ decreases from 2 to $1\,\mathrm{fm}^{-1}$). When initial 3NFs are included, a similar pattern is found, but the decrease is more nucleus dependent and larger by as much as a factor of 2 (i.e., up to about $2\,\mathrm{MeV}$). This increase in binding is consistent with the difference in running between NN+NNN-induced and NN+NNN observed for ^{12}C in Ref. [18] with the same interactions.

Results with 3NFs for higher λ are consistent with small changes, but the uncertainties after extrapolation are too large to be definitive. In contrast, Roth et al. found a steady linear increase in binding from λ above $2.2\,\mathrm{fm}^{-1}$ down to $1.6\,\mathrm{fm}^{-1}$ for ^{12}C [18]. This is not evident in the systematics of the central values of our extrapolations, but possible within the estimated error bars. It would be most helpful to have accurate energy calculations for the initial Hamiltonian to fully assess the degree of running down to $\lambda = 2\,\mathrm{fm}^{-1}$. For excited states we also find similar quantitative differences between NN+NNN-induced and NN+NNN calculations and for some particular states there are qualitative differences.

Further investigations are warranted. For example, it will be important to compare our present results, which use harmonic oscillator evolved SRG 3NFs, to forthcoming calculations using the same initial interactions but evolved in momentum space using recently developed SRG technology [20]. Further explorations at low λ will help to map out the quantitative scaling of induced 4NF contributions. Improved convergence at these low resolutions motivates searching for simple approximations to account for these 4NF contributions to the energy and other observables. Besides additional CI calculations, application of highly evolved two- and three-nucleon forces may also be fruitful for coupled cluster [43] methods, *ab initio* density functional theory [44], and NCSM/RGM [5, 45–48] calculations of light nuclear reactions.

Our studies were limited in basis size by the available codes and computer resources. We anticipate further developments in improved basis construction and evolution algorithms. We could also study non-oscillator

basis spaces [49, 50] and apply the importance truncation technique [17] to increase available basis sizes. We look forward to a detailed extrapolation analysis of such results. In addition, a difficulty encountered here with an insufficient initial $A = 3$ basis at smaller $\hbar\Omega$ (see Section III A) might be circumvented by the momentum-space evolution technology [20], so that matrix elements in the oscillator basis are only calculated *after* evolution.

We considered only a single initial NN+NNN Hamiltonian in our analysis. While in past investigations [16] other choices of initial NN Hamiltonians have displayed no qualitative difference in the effects of the SRG procedure, studies with a range of Hamiltonians are highly desirable. It will also be important to consider consistent operators for other observables. In this regard, new extrapolation methods for radii and other long-distance operators may be particularly valuable [34].

Our results demonstrate a level of precision in induced many-body force effects that allows further analysis of the impact of additional χEFT inputs. In all cases presented here the addition of 3NFs from the initial χEFT Hamiltonian overbinds the ground states. Our results suggest that the effects of missing induced forces due to softening transformations are small (at least in larger nuclei) compared to discrepancies with experiment. These discrepancies may be reduced by additional 3NF and 4NF contributions at N^{3}LO in the χEFT. Suitable matrix elements of these terms will be available for calculations in the near future and it will be important to incorporate them.

[1] P. Maris, J. P. Vary, and A. M. Shirokov, Phys. Rev. C **79**, 014308 (2009).

[2] P. Navratil, S. Quaglioni, I. Stetcu, and B. R. Barrett, J. Phys. G **36**, 083101 (2009).

[3] P. Maris, A. M. Shirokov, and J. P. Vary, Phys. Rev. C **81**, 021301 (2010).

[4] P. Maris, J. P. Vary, P. Navratil, W. E. Ormand, H. Nam, and D. J. Dean, Phys. Rev. Lett. **106**, 202502 (2011).

[5] P. Navratil and S. Quaglioni, Phys. Rev. Lett. **108**, 042503 (2012).

[6] B. R. Barrett, P. Navratil, and J. P. Vary, Prog. Part. Nucl. Phys. **69**, 131 (2013).

[7] S. D. Glazek and K. G. Wilson, Phys. Rev. D **48**, 5863 (1993).

[8] F. Wegner, Ann. Phys. **506**, 77 (1994).

[9] S. K. Bogner, R. J. Furnstahl, and A. Schwenk, Prog. Part. Nucl. Phys. **65**, 94 (2010).

[10] R. J. Furnstahl, Nucl. Phys. Proc. Suppl. **228**, 139 (2012).

[11] S. K. Bogner, R. J. Furnstahl, and R. J. Perry, Phys. Rev. C **75**, 061001 (2007).

[12] S. K. Bogner, R. J. Furnstahl, R. J. Perry, and A. Schwenk, Phys. Lett. B **649**, 488 (2007).

[13] E. D. Jurgenson, S. K. Bogner, R. J. Furnstahl, and R. J. Perry, Phys. Rev. C **78**, 014003 (2008).

[14] S. K. Bogner, R. J. Furnstahl, P. Maris, R. J. Perry, A. Schwenk, and J. P. Vary, Nucl. Phys. A **801**, 21 (2008).

[15] E. D. Jurgenson, P. Navratil, and R. J. Furnstahl, Phys. Rev. Lett. **103**, 082501 (2009).

[16] E. D. Jurgenson, P. Navratil, and R. J. Furnstahl, Phys. Rev. C **83**, 034301 (2011).

[17] R. Roth, Phys. Rev. C **79**, 064324 (2009).

[18] R. Roth, J. Langhammer, A. Calci, S. Binder, and P. Navratil, Phys. Rev. Lett. **107**, 072501 (2011).

[19] R. Roth, S. Binder, K. Vobig, A. Calci, J. Langhammer, and P. Navratil, Phys. Rev. Lett. **109**, 052501 (2012).

[20] K. Hebeler, Phys. Rev. C **85**, 021002 (2012).

[21] D. R. Entem and R. Machleidt, Phys. Rev. C **68**, 041001 (2003).

[22] E. Epelbaum, A. Nogga, W. Gloeckle, H. Kamada, U.-G. Meissner, and H. Witala, Phys. Rev. C **66**, 064001 (2002).

[23] P. Navratil, Few Body Syst. **41**, 117 (2007).

[24] P. Navratil, V. G. Gueorguiev, J. P. Vary, W. E. Ormand, and A. Nogga, Phys. Rev. Lett. **99**, 042501 (2007).

[25] S. Kehrein, *The Flow Equation Approach to Many-Particle Systems* (Springer, Berlin, 2006).

[26] E. R. Anderson *et al.*, Phys. Rev. C **77**, 037001 (2008).

[27] W. Li, E. R. Anderson, and R. J. Furnstahl, Phys. Rev. C **84**, 054002 (2011).

[28] E. D. Jurgenson and R. J. Furnstahl, Nucl. Phys. A **818**, 152 (2009).

[29] D. Gazit, S. Quaglioni, and P. Navratil, Phys. Rev. Lett. **103**, 102502 (2009).

[30] P. Sternberg, E. G. Ng, C. Yang, P. Maris, J. P. Vary, M. Sosonkina, and H. V. Le, in *Proceedings of the 2008 ACM/IEEE conference on Supercomputing*, SC '08 (IEEE Press, Piscataway, NJ, USA, 2008) pp. 15:1–15:12.

[31] P. Maris, M. Sosonkina, J. P. Vary, E. G. Ng, and C. Yang, Procedia CS **1**, 97 (2010).

[32] H. M. Aktulga, C. Yang, E. G. Ng, P. Maris, and J. P. Vary, in *Euro-Par*, Lecture Notes in Computer Science, Vol. 7484, edited by C. Kaklamanis, T. S. Papatheodorou, and P. G. Spirakis (Springer, 2012) pp. 830–842.

[33] P. Maris, H. Aktulga, M. A. Caprio, U. Çatalyürek, E. Ng, D. Oryspayev, H. Potter, E. Saule, M. Sosonkina, J. Vary, C. Yang, and Z. Zhou, J. Phys. Conf. Ser. **403**, 012019 (2012).

[34] R. J. Furnstahl, G. Hagen, and T. Papenbrock, Phys. Rev. C **86**, 031301 (2012).

[35] S. A. Coon, M. I. Avetian, M. K. G. Kruse, U. van Kolck, P. Maris, and J. P. Vary, Phys. Rev. C **86**, 054002 (2012).

[36] S. More, A. Ekström, R. J. Furnstahl, G. Hagen, and T. Papenbrock, (2013).

[37] A. Calci, J. Langhammer, P. Maris, R. Roth, and J. Vary, (2013), in preparation.

[38] C. Cockrell, J. P. Vary, and P. Maris, Phys. Rev. C **86**, 034325 (2012).

[39] E. Epelbaum, H.-W. Hammer, and U.-G. Meissner, Rev. Mod. Phys. **81**, 1773 (2009).

[40] M. A. Caprio, P. Maris, and J. P. Vary, Phys. Lett. **B719**, 179 (2013).

[41] L. E. Marcucci, M. Pervin, S. C. Pieper, R. Schiavilla, and R. B. Wiringa, Phys. Rev. C **78**, 065501 (2008).

[42] S. Pastore, S. C. Pieper, R. Schiavilla, and R. Wiringa, (2012).

[43] G. Hagen, D. J. Dean, M. Hjorth-Jensen, T. Papenbrock, and A. Schwenk, Phys. Rev. C **76**, 044305 (2007).

[44] J. E. Drut and L. Platter, Phys. Rev. C **84**, 014318 (2011).

[45] S. Quaglioni and P. Navratil, Phys. Rev. Lett. **101**, 092501 (2008).

[46] P. Navratil, R. Roth, and S. Quaglioni, Phys. Rev. C **82**, 034609 (2010).

[47] P. Navratil, R. Roth, and S. Quaglioni, Phys.Lett. **B704**, 379 (2011).

[48] S. Quaglioni, P. Navratil, R. Roth, and W. Horiuchi, (2012), arXiv:1203.0268 [nucl-th].

[49] M. A. Caprio, P. Maris, and J. P. Vary, Phys. Rev. C **86**, 034312 (2012).

[50] M. Caprio, P. Maris, and J. P. Vary, J. Phys. Conf. Ser. **403**, 012014 (2012).